J. Fluid Mech. (1996), *vol.* 323, *pp.* 173–200

Lateral vorticity measurements in a turbulent wake

By R. A. ANTONIA, Y. ZHU AND H. S. SHAFI

Department of Mechanical Engineering, University of Newcastle, NSW, 2308, Australia

(Received 28 June 1995 and in revised form 19 April 1996)

The accurate measurement of vorticity has proven difficult because of the difficulty of estimating spatial derivatives of velocity fluctuations reliably. A method is proposed for correcting the lateral vorticity spectrum measured using a four-wire probe. The attenuation of the measured spectrum increases as the wavenumber increases but does not vanish when the wavenumber is zero. Although the correction procedure assumes local isotropy, the major contributor to the high-wavenumber part of the vorticity spectrum is the streamwise derivative of the lateral velocity fluctuation, and the correction of this latter quantity does not depend on local isotropy. Satisfactory support for local isotropy is provided by the high-wavenumber parts of the velocity, velocity derivative and vorticity spectra measured on the centreline of a turbulent wake. Second- and fourth-order moments of vorticity show departures from local isotropy but the degree of departure seems unaffected by the turbulence Reynolds number R_λ. The vorticity probability density function is approximately exponential and has tails which stretch out to larger amplitudes as R_λ increases. The vorticity flatness factor, which is appreciably larger than the flatness factor of the streamwise velocity derivative, also increases with R_λ. When R_λ is sufficiently large for velocity structure functions to indicate a $r^{2/3}$ inertial range, two-point longitudinal correlations of lateral vorticity fluctuations give encouraging support for the theoretical $r^{-4/3}$ behaviour.

1. Introduction

Vorticity, or the measure of rotation of a fluid element, is an important defining characteristic of turbulence. It is not therefore surprising that there have been a number of attempts, using various methods, to measure it (see, for example, Corrsin & Kistler 1955; Foss 1979; Van Atta 1979; Willmarth 1979; Wallace 1986; Foss & Wallace 1989). Measurements of either one, two or, in a few instances, all three components of the vorticity vector ω_i ($\equiv \epsilon_{ijk} u_{k,j}$, where ϵ_{ijk} is the alternating tensor and $u_{k,j} \equiv \partial u_k / \partial x_j$; standard tensor notation applies) have been reported in different flows. Earlier measurements of ω_1, using a four-sensor hot-wire probe (Kovasznay 1954) were made in a rough-wall turbulent boundary layer (Corrsin & Kistler 1955). Later, a modified Kovasznay probe (Kastrinakis, Eckelmann & Willmarth 1979) was used for ω_1 measurements in a turbulent boundary layer (Wallace & Vukoslavcevic 1982) and a fully developed turbulent channel flow (Kastrinakis & Eckelmann 1983). More recently, this type of probe was used for ω_1 measurements in laboratory-grid, boundary layer and wake flows as well as the atmospheric surface layer (Fan 1991). Statistics of all three components of ω_i have been obtained with a nine-sensor hot-wire probe in a mixing layer (Balint, Wallace & Vukoslavcevic 1989) and a boundary

layer (Balint, Wallace & Vukoslavcevic 1991), a twelve-sensor hot-wire probe in grid and boundary layer flows (Tsinober, Kit & Dracos 1992) and the intermediate wake of a circular cylinder (Marasli, Nguyen & Wallace 1993) and a twenty-sensor hot-wire probe (Lemonis 1995) in grid and boundary layer flows.

As well as being an obvious candidate for providing information on the vortical flow (e.g. through two-point vorticity correlations or conditional velocity–vorticity correlations: Wallace 1986; Ong 1992; Rajagopalan & Antonia 1993), vorticity data also allow properties of the small-scale structure of turbulence to be studied. Spectra of the mean-square vorticity or enstrophy ($\frac{1}{2}\overline{\omega^2} \equiv \frac{1}{2}\overline{\omega_i\omega_i}$) contain relatively higher wavenumber energy than the velocity or turbulent kinetic energy spectra (Antonia, Shah & Browne 1988*b*; Balint *et al.* 1991; evidence for this will also be presented later in this paper). Naturally, the separation between the peaks of these two spectra increases with the Reynolds number.

Corrsin & Kistler (1955) pointed out that vorticity-dominated phenomena must be associated with the fine structure of the turbulence. This association raises the question of how closely the statistics of ω_i conform with local isotropy. It also raises the issue of how these statistics depend on the turbulence Reynolds number R_λ ($\equiv \overline{u_1^2}^{1/2}\lambda/\nu$, where u_1 is the velocity fluctuation in the x_1 direction, λ is the Taylor microscale $\overline{u_1^2}^{1/2}/\overline{u_{1,1}^2}^{1/2}$ and ν is the kinematic viscosity of the fluid). Although several studies have presented results of vorticity statistics (e.g. Meneveau *et al.* 1990; Fan 1991; Marasli *et al.* 1993; Mi & Antonia 1996), progress on the previous two questions has been slow, primarily because of the difficulty of measuring the high-wavenumber part of the vorticity spectrum reliably. When hot-wire anemometry is used, the measurement of ω_i invariably involves the use of multiple hot wires so that the effect of the spatial resolution of the probe needs to be taken into account. Several studies have examined the effect of spatial resolution on the measurement of vorticity or its components (e.g. Wyngaard 1968,1969; Antonia, Zhu & Kim 1993; Zhu, Antonia & Kim 1993; Zhu & Antonia 1995*a*,*b*; see also the review by Wallace & Foss 1995). Although Wyngaard (1969) has analysed the spatial resolution of the Kovasznay-type ω_1 probe, no corresponding analysis is available for ω_2 and ω_3 probes.

The first objective of this paper is to quantify the effect of spatial resolution on the measurement of ω_i ($i = 2, 3$) using a relatively simple probe configuration. A procedure for correcting the high-wavenumber part of the vorticity spectrum is developed and applied to the data. This methodology is important since it leads to corrected vorticity spectra and, after integration, corrected vorticity variances. Indeed, the second aim of the paper is to compare the statistics of vorticity with local isotropy and examine the dependence of these statistics on the turbulence Reynolds number. A consequence of local isotropy is the $r^{-4/3}$ behaviour of two-point vorticity correlations, when the separation falls in the inertial range. Such a behaviour has not previously been experimentally verified. The data have been collected in the same flow to avoid the possibility that different flows may have different levels of (large scale) anisotropy which could, in turn, affect the small-scale statistics. The flow chosen for the present work is the turbulent wake of a circular cylinder. There were two main reasons for this choice. First, the turbulence level is relatively low (typically less than $6 \sim 7\%$), justifying the use of Taylor's hypothesis. Secondly, the magnitude of the Kolmogorov length scale is sufficiently large (typically $0.2 \sim 0.4$ mm) to allow spatial resolution effects to be studied. The largest value ($\simeq 260$) for R_λ is sufficient for an inertial range to be observed.

The spatial resolution of the vorticity probe is considered in §2. Some of the

consequences of local isotropy are presented in §3, while §4 gives details of the flow and the instrumentation used. Vorticity statistics are compared with local isotropy in §5. The Reynolds number dependence of the statistics is discussed in §6. In §7, we provide some evidence for the inertial-range behaviour of two-point vorticity correlations. In §8, the present results are compared with those obtained in other flows.

2. Correction procedure for lateral vorticity components

The effect that too large a separation between parallel hot wires can have on the high-wavenumber part of the spatial derivative spectrum ($\phi_{u_{1,2}}$ or $\phi_{u_{1,3}}$) has been quantified in the literature (e.g. Wyngaard 1969; Antonia, Browne & Chambers 1984; Antonia *et al.* 1993; Ewing, Hussein & George 1995) both analytically and experimentally. Wyngaard's analysis (1968,1969) provides a useful method of correcting for the high-wavenumber spectral attenuation. With slight modifications (e.g. Antonia & Mi, 1993*a*), the approach has been tested with DNS data for $u_{1,2}$ and other spatial velocity derivatives (Antonia *et al.* 1993; Antonia, Zhu & Kim 1994; Zhu & Antonia 1995*a*). It can, in principle, be applied to any configuration, including the relatively complicated hot-wire arrangements used in vorticity probes. Wyngaard (1969) presented analyses of the spatial resolution of arrays for measuring velocity derivatives and of the Kovasznay ω_1 probe. A correction procedure for ω_3 is outlined below (a similar treatment could be developed for ω_2). By definition,

$$\omega_3 = u_{2,1} - u_{1,2} \quad . \tag{2.1}$$

The variance of ω_3 is given by

$$\overline{\omega_3^2} = \overline{u_{2,1}^2} + \overline{u_{1,2}^2} - 2\overline{u_{1,2}u_{2,1}} \quad . \tag{2.2}$$

The accuracy of estimating $\overline{\omega_3^2}$ will depend on the accuracy with which the terms $\overline{u_{2,1}^2}$, $\overline{u_{1,2}^2}$ and $\overline{u_{1,2}u_{2,1}}$ can be measured. Alternatively, the accuracy of ϕ_{ω_3}, the spectrum of ω_3, will depend on that of $\phi_{u_{2,1}}$, $\phi_{u_{1,2}}$ and of the cospectrum $Co_{u_{1,2}u_{2,1}}$.

Multiple wires, necessarily displaced from one another in space, are used in a vorticity probe. Consequently, the velocity components are measured at slightly different spatial locations. This, in addition to the finite wire lengths, means that it is important to distinguish between measured and true values of velocities, velocity derivatives and vorticities so as to account for the finite spatial resolution of the probe (e.g. Silverman 1968; Wyngaard 1969). Measured quantities will be denoted by a superscript m; no superscripts will be used when referring to the true values.

The quantities $u_{2,1}^m$ and $u_{1,2}^m$ can, in general, be expressed as follows:

$$u_{2,1}^m = \int_{-\infty}^{\infty} \mathrm{e}^{\mathrm{i}\boldsymbol{k}\cdot\boldsymbol{x}} \mathrm{d}\boldsymbol{Z}_{21}^m, \tag{2.3}$$

$$u_{1,2}^m = \int_{-\infty}^{\infty} \mathrm{e}^{\mathrm{i}\boldsymbol{k}\cdot\boldsymbol{x}} \mathrm{d}\boldsymbol{Z}_{12}^m, \tag{2.4}$$

where $\mathrm{d}\boldsymbol{Z}_{21}$ and $\mathrm{d}\boldsymbol{Z}_{12}$ are the Fourier–Stieltjes components of $u_{2,1}$ and $u_{1,2}$ respectively, $\boldsymbol{k}$ is the wavenumber vector with magnitude $k \equiv (k_1^2+k_2^2+k_3^2)^{1/2}$. The measured spectra of $u_{2,1}$, $u_{1,2}$ and their cospectrum may be expressed as

$$\phi_{u_{2,1}}^m(\boldsymbol{k})\mathrm{d}\boldsymbol{k} = \overline{\mathrm{d}\boldsymbol{Z}_{21}^m(\mathrm{d}\boldsymbol{Z}_{21}^m)^\dagger}, \tag{2.5}$$

$$\phi^m_{u_{1,2}}(\boldsymbol{k})\mathrm{d}\boldsymbol{k} = \overline{\mathrm{d}\boldsymbol{Z}^m_{12}(\mathrm{d}\boldsymbol{Z}^m_{12})^\dagger}, \tag{2.6}$$

$$Co^m_{u_{1,2}u_{2,1}}(\boldsymbol{k})\mathrm{d}\boldsymbol{k} = \overline{\mathrm{d}\boldsymbol{Z}^m_{12}(\mathrm{d}\boldsymbol{Z}^m_{21})^\dagger}, \tag{2.7}$$

where the dagger denotes a complex conjugate. The 'true' spectra and cospectra may be written, in general, as

$$\phi_{u_{2,1}}(\boldsymbol{k}) = k_1^2\phi_{22}(\boldsymbol{k}), \tag{2.8}$$

$$\phi_{u_{1,2}}(\boldsymbol{k}) = k_2^2\phi_{11}(\boldsymbol{k}), \tag{2.9}$$

$$Co_{u_{1,2}u_{2,1}}(\boldsymbol{k}) = k_1k_2\phi_{12}(\boldsymbol{k}). \tag{2.10}$$

Equation (2.10) follows from the more general expression

$$Co_{u_{i,m}u_{j,n}}(\boldsymbol{k}) = k_mk_n\phi_{ij}(\boldsymbol{k}),$$

where $\phi_{ij}(\boldsymbol{k})$ is the energy spectrum tensor. For isotropic turbulence (Batchelor 1953, p. 49),

$$\phi_{ij}(\boldsymbol{k}) = \phi_{ij}(k) = \frac{E(k)}{4\pi k^4}(k^2\delta_{ij} - k_ik_j) \tag{2.11}$$

where $E(k)$ is the three-dimensional energy spectrum.

With this simplification, the ratios of the measured one-dimensional spectra $\phi^m_{u_{2,1}}(k_1)$, $\phi^m_{u_{1,2}}(k_1)$ and cospectrum $Co^m_{u_{1,2}u_{2,1}}(k_1)$ and their true values

$$\frac{\phi^m_{u_{2,1}}(k_1)}{\phi_{u_{2,1}}(k_1)} = \iint_{-\infty}^{\infty}\phi^m_{u_{2,1}}(k)\mathrm{d}k_2\mathrm{d}k_3 \Big/ \iint_{-\infty}^{\infty}\phi_{u_{2,1}}(k)\mathrm{d}k_2\mathrm{d}k_3, \tag{2.12}$$

$$\frac{\phi^m_{u_{1,2}}(k_1)}{\phi_{u_{1,2}}(k_1)} = \iint_{-\infty}^{\infty}\phi^m_{u_{1,2}}(k)\mathrm{d}k_2\mathrm{d}k_3 \Big/ \iint_{-\infty}^{\infty}\phi_{u_{1,2}}(k)\mathrm{d}k_2\mathrm{d}k_3, \tag{2.13}$$

$$\frac{Co^m_{u_{1,2}u_{2,1}}(k_1)}{Co_{u_{1,2}u_{2,1}}(k_1)} = \iint_{-\infty}^{\infty}Co^m_{u_{1,2}u_{2,1}}(k)\mathrm{d}k_2\mathrm{d}k_3 \Big/ \iint_{-\infty}^{\infty}Co_{u_{1,2}u_{2,1}}(k)\mathrm{d}k_2\mathrm{d}k_3 \tag{2.14}$$

can be estimated for any value of k_1 by numerically evaluating the double integrals in (2.12)–(2.14). The ratio $\phi^m_{\omega_3}(k_1)/\phi_{\omega_3}(k_1)$ can also be estimated since

$$\phi_{\omega_3}(k_1) = \phi_{u_{2,1}}(k_1) + \phi_{u_{1,2}}(k_1) - 2Co_{u_{1,2}u_{2,1}}(k_1). \tag{2.15}$$

Before the numerator in (2.12)–(2.14) can be estimated, the coefficients $\mathrm{d}\boldsymbol{Z}^m_{21}$ and $\mathrm{d}\boldsymbol{Z}^m_{12}$ in (2.5)–(2.7) need to be expressed in terms of the geometrical parameters (e.g. separations between the hot wires, their effective lengths and inclinations) of the particular probe used.

Different probe configurations have been used in the literature (e.g. Foss 1979; Haw, Foss & Foss 1988; Klewicki & Falco 1990; Antonia & Rajagopalan 1990; Rajagopalan & Antonia 1993). Here we focus on one probe configuration (figure 1*a*). The probe consists of one X-wire which straddles parallel single hot wires; this configuration was used by Haw *et al.* (1988), Antonia & Rajagopalan (1990) and Rajagopalan & Antonia (1993). The single wires are used to infer the streamwise component of velocity, i.e. it is assumed that the single wires respond only to U_1 and not to $(U_1^2 + U_2^2)^{1/2}$. Expressions for $\phi^m_{u_{1,2}}$, $\phi^m_{u_{2,1}}$, $Co^m_{u_{1,2}u_{2,1}}$ and $\phi^m_{\omega_3}$ in terms of the geometrical parameters of the probe are given in the Appendix. The ratio $\phi^m_{\omega_3}(k)/\phi_{\omega_3}(k_1)$ as well as the ratios in (2.12)–(2.14) are shown in figure 2. The streamwise separation $\Delta x_1^* = -\overline{U}_1\Delta t/\eta$ which corresponds to the time Δt between samples ($\Delta t \equiv f_s^{-1}$, where f_s is the sampling frequency of the data acquisition; $\overline{U}_1$ is

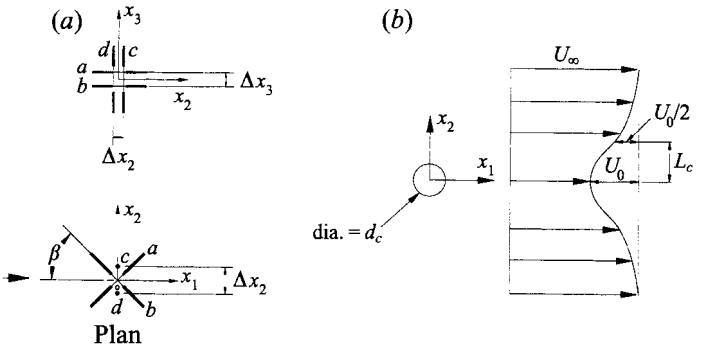

FIGURE 1. (*a*) Probe geometry used for the measurement of ω_2 or ω_3. (*b*) Definition sketch of the flow and coordinate system.

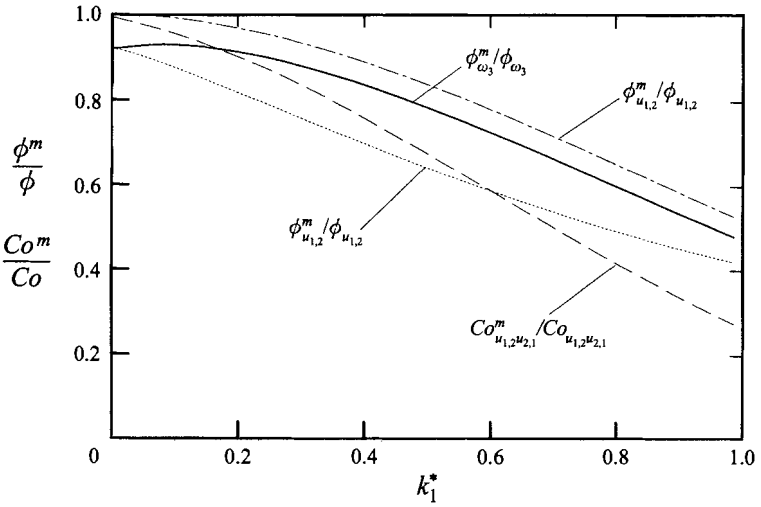

FIGURE 2. Spectral correction ratios for ω_3^m and its components. $\Delta x_1^* = 2$, $\Delta x_2^* = 4$, $\Delta x_3^* = 2$, $l^* = 2$, $\beta = 45°$.

the local mean streamwise velocity) was equal to 2. The values of Δx_2^* (the distance between the parallel hot wires), Δx_3^* (the spanwise distance between the wires of X-probe), the wire length l^* and the effective angle β (or $\pi - \beta$) of the X-wires were 4, 2, 2 and 45° respectively. (The asterisk denotes normalization by the Kolmogorov length scale $\eta \equiv \nu^{3/4}/\bar{\epsilon}^{1/4}$ and velocity scale $U_K \equiv \nu^{1/4}\bar{\epsilon}^{1/4}$ where ν is the kinematic viscosity of the fluid and $\bar{\epsilon}$ is the mean turbulent energy dissipation rate.)

Notwithstanding the relatively small values chosen for Δx_2^*, Δx_3^* and Δx_1^*, figure 2 shows that the spectral corrections that need to be applied to the measured ω_3 spectrum are not negligible. As expected, the magnitude of the correction increases as k_1^* approaches unity. For $k_1^* = 1$, the attenuation in $\phi_{\omega_3}^m$ is about 40%. The attenuation is not negligible at small wavenumbers, even at $k_1^* = 0$ where it is of order 10%. This behaviour was also noted by Wyngaard & Pao (1972). The finite attenuation at small wavenumbers is caused by the attenuation of $\phi_{u_{1,2}}$ and $Co_{u_{1,2}u_{2,1}}$; the formation of the ratio $\phi_{u_{1,2}}^m(k_1)/\phi_{u_{1,2}}(k_1)$ requires integration over all values of k_2 and k_3 (for convenience, the wire length effect has been ignored and only the separation Δx_2

between the parallel hot wires is included):

$$\frac{\phi^m_{u_{1,2}}(k_1)}{\phi_{u_{1,2}}(k_1)} = \frac{4\iint_{-\infty}^{\infty} \sin^2\left(\frac{k_2\Delta x_2}{2}\right)\frac{E(k)}{4\pi k^4}(k^2-k_1^2)\mathrm{d}k_2\mathrm{d}k_3}{(\Delta x_2)^2\iint_{-\infty}^{\infty} k_2^2\frac{E(k)}{4\pi k^4}(k^2-k_1^2)\mathrm{d}k_2\mathrm{d}k_3}\,. \tag{2.16}$$

The ratio will remain less than 1 for all values of k_1. In other words, the spectrum of vorticity is attenuated at all wavenumbers. Wyngaard & Pao attributed this to the fact that, unlike the three-dimensional velocity spectrum, the 'effective' three-dimensional vorticity spectrum has a positive slope in the inertial range; this means that small scales are likely to contribute significantly at all k_1.

An appropriate way of testing the validity of the correction technique would be to measure $\overline{\omega_3^2}$ with different values of Δx_i^*, apply the correction scheme and compare the results. Since changing the relative configurations of the wires of the present probe without breaking the wires is extremely tedious, an alternative test would be to apply the scheme to individual components of $\overline{\omega_3^2}$. In a previous investigation (Zhu *et al.* 1993), the correction scheme was tested for $\overline{u_{1,2}^2}$, as measured using two parallel hot wires in a fully developed turbulent channel flow. The corrected values of $\overline{u_{1,2}^2}$ compared favourably with estimates obtained from the correlation method and also with DNS data for $\overline{u_{1,2}^2}$ in the same flow (and Reynolds number). The correction procedure was also applied to DNS data for $u_{1,2}$, evaluated with a central finite difference scheme similar to that used in the experiment (Antonia *et al.* 1993); other spatial velocity derivatives were considered in Antonia *et al.* (1994). The results provide important corroboration of the procedure, at least when local isotropy is satisfied.

While the assumption of local isotropy is necessary for the practical implementation of the procedure, it is important to underline that the correction of $\phi_{u_{2,1}}$ (or indeed the spectrum of any streamwise derivative) does not require this assumption. The ratio $\phi^m_{u_{2,1}}(k_1)/\phi_{u_{2,1}}(k_1)$ reduces to

$$\frac{\phi^m_{u_{2,1}}(k_1)}{\phi_{u_{2,1}}(k_1)} = \frac{\sin^2\left(\frac{1}{2}k_1\Delta x_1\right)}{\left(\frac{1}{2}k_1\Delta x_1\right)^2}\,. \tag{2.17}$$

The formation of this ratio requires neither the assumption of isotropy nor any knowledge of $E(k)$. As shown in figure 2, the ratio in (2.17) approaches 1 when $k_1^* \to 0$. The correction procedure for $\overline{u_{2,1}^2}$ was tested using the data from two X-wire probes in a wake flow (Zhu & Antonia 1995*a*; Mi & Antonia 1996). After correction, the $\phi_{u_{2,1}}$ distributions for different Δx_1^* values were indistinguishable from each other, thus validating the correction scheme for $\phi_{u_{2,1}}$. The procedure has not been checked for $Co_{u_{1,2}u_{2,1}}$ for the present probe geometry. Since its contribution to ϕ_{ω_3} (or $\overline{\omega_3^2}$) is relatively small (this can be seen in §5), it seems natural to expect that any error in correcting $Co_{u_{1,2}u_{2,1}}$, will only have a small effect on ϕ_{ω_3} (or $\overline{\omega_3^2}$). Further validation of the correction scheme was obtained by applying it to two X-wires separated in a lateral direction (Zhu & Antonia 1995*a*; Mi & Antonia 1996). Measurements in the wake flow with different separations between the X-wires yielded essentially the same value of $\overline{\omega_3^2}$, after the application of the correction (Mi & Antonia 1996).

Figure 2 indicates that $\phi_{u_{1,2}}$ and $Co_{u_{1,2}u_{2,1}}$ are much more attenuated than $\phi_{u_{2,1}}$; although this is important when correcting the low-wavenumber region of ϕ_{ω_3}, it will

be shown in §5 that $\phi_{u_{2,1}}$ provides the major contribution to the high-wavenumber part of ϕ_{ω_3}. In this context, the correction that is applied to the measured ω_3 (or ω_2) spectrum should not invalidate the comparison of the high-wavenumber part of the corrected spectrum with isotropy; isotropic relations for the vorticity spectra are given in the following section.

3. Local isotropy

Since velocity derivatives give more weight to the high-wavenumber part of the spectrum than velocity fluctuations (Corrsin & Kistler 1955; Antonia, Anselmet & Chambers 1986; Balint *et al.* 1991; Van Atta 1991), ω_i should in principle provide a better test for local isotropy than u_i. (The DNS data for vorticity and velocity spectra tend to support this expectation, Antonia & Kim 1994.) In this section, we consider the consequences of isotropy on the moments and spectra of ω_i at one point in space. (Two-point correlations are considered in §7.)

Second-order moments of ω_i are equal:

$$\overline{\omega_1^2} = \overline{\omega_2^2} = \overline{\omega_3^2} = 5\overline{u_{1,1}^2}\,, \tag{3.1}$$

a result which follows from the isotropic relation (e.g. Antonia, Browne & Shah 1988*a*)

$$\overline{u_{i,j}u_{k,m}} = \tfrac{1}{2}\overline{u_{1,1}^2}(4\delta_{ik}\delta_{jm} - \delta_{ij}\delta_{km} - \delta_{im}\delta_{jk})\,. \tag{3.2}$$

Relations for the components of $\overline{\omega_2^2}$ and $\overline{\omega_3^2}$ also follow from (3.2):

$$\left.\begin{aligned} \overline{u_{1,2}^2} = \overline{u_{1,3}^2} = \overline{u_{2,1}^2} = \overline{u_{3,1}^2} = 2\overline{u_{1,1}^2}, \\ -\overline{u_{1,2}u_{2,1}} = -\overline{u_{1,3}u_{3,1}} = \tfrac{1}{2}\overline{u_{1,1}^2}. \end{aligned}\right\} \tag{3.3}$$

Odd-order moments of ω_i should be zero by virtue of the symmetry of vorticity probability density function $p(\omega_i)$; the isotropic form of the sixth-order tensor (equation (A4) in Champagne 1978) can be shown to satisfy $\overline{\omega_1^3} = \overline{\omega_2^3} = \overline{\omega_3^3} = 0$. Consequently, the skewnesses S_{ω_i} (e.g. $S_{\omega_1} = \overline{\omega_1^3}/\overline{\omega_1^2}^{3/2}$) should all be zero, i.e.

$$S_{\omega_1} = S_{\omega_2} = S_{\omega_3} = 0\,. \tag{3.4}$$

The isotropic relation between the components of $\overline{\omega_i^4}$ can be obtained from the eighth-order velocity gradient correlation function. An expression for this function was obtained by Phan-Thien & Antonia (1994) after first deriving a recursive relation for the unit isotropic tensor of arbitrary even order and using symmetry and incompressibility to reduce it to

$$\begin{aligned} \overline{u_{i,m}u_{j,n}u_{k,p}u_{l,q}} = \tfrac{1}{12}\overline{u_{1,1}^4}\{25\,(\delta_{ij}\delta_{mn}\delta_{kl}\delta_{pq} + \delta_{ik}\delta_{mp}\delta_{jl}\delta_{nq} + \delta_{il}\delta_{mq}\delta_{jk}\delta_{np}) \\ - 5\,[\delta_{ij}\delta_{mn}\,(\delta_{kl}\delta_{pq} + \delta_{kp}\delta_{lq} + \delta_{kq}\delta_{lp}) \\ + \delta_{ik}\delta_{mp}\,(\delta_{jl}\delta_{nq} + \delta_{jn}\delta_{lq} + \delta_{jq}\delta_{ln}) \\ + \delta_{il}\delta_{mq}\,(\delta_{jk}\delta_{np} + \delta_{jn}\delta_{kp} + \delta_{jp}\delta_{kn}) \\ + \delta_{jk}\delta_{np}\,(\delta_{il}\delta_{mq} + \delta_{im}\delta_{lq} + \delta_{iq}\delta_{lm}) \\ + \delta_{jl}\delta_{nq}\,(\delta_{ik}\delta_{mp} + \delta_{im}\delta_{kp} + \delta_{ip}\delta_{km}) \\ + \delta_{kl}\delta_{pq}\,(\delta_{ij}\delta_{mn} + \delta_{im}\delta_{jn} + \delta_{in}\delta_{jm})] \end{aligned}$$

$$+ \left(\delta_{ij}\delta_{mn} + \delta_{im}\delta_{jn} + \delta_{in}\delta_{jm}\right)\left(\delta_{kl}\delta_{pq} + \delta_{kp}\delta_{lq} + \delta_{kq}\delta_{lp}\right)$$
$$+ \left(\delta_{ik}\delta_{mp} + \delta_{im}\delta_{kp} + \delta_{ip}\delta_{km}\right)\left(\delta_{jl}\delta_{nq} + \delta_{jn}\delta_{lq} + \delta_{jq}\delta_{ln}\right)$$
$$+ \left(\delta_{il}\delta_{mq} + \delta_{im}\delta_{lq} + \delta_{iq}\delta_{lm}\right)\left(\delta_{jk}\delta_{np} + \delta_{jn}\delta_{kp} + \delta_{jp}\delta_{kn}\right)\Big\} . \quad (3.5)$$

Siggia (1981) expressed the fourth-order velocity derivative tensor in isotropic turbulence in terms of four invariants; these invariants may be expressed in terms of $\overline{u_{1,1}^4}$ only. One consequence of (3.5) is

$$\overline{\omega_1^4} = \overline{\omega_2^4} = \overline{\omega_3^4} = 25\overline{u_{1,1}^4} . \quad (3.6)$$

It follows from (3.1) and (3.6) that the flatness factors F_{ω_i} (e.g. $F_{\omega_1} = \overline{\omega_1^4}/\overline{\omega_1^2}^2$) are all equal, with the same magnitude as the flatness factor of $u_{1,1}$, namely

$$F_{\omega_1} = F_{\omega_2} = F_{\omega_3} = F_{u_{1,1}} . \quad (3.7)$$

The flatness factors of the main components of ω_2 and ω_3 are also equal to $F_{u_{1,1}}$, namely

$$F_{u_{2,1}} = F_{u_{3,1}} = F_{u_{1,2}} = F_{u_{1,3}} = F_{u_{1,1}}. \quad (3.8)$$

Because of the solenoidality of ω_i and u_i (Batchelor 1953; Monin & Yaglom 1975; Antonia & Kim 1994), isotropic relations between vorticity spectra have the same form as isotropic relations between velocity spectra, namely

$$\phi_{u_2}(k_1) = \phi_{u_3}(k_1) = \frac{1}{2}\left(\phi_{u_1} - k_1\frac{\partial\phi_{u_1}}{\partial k_1}\right), \quad (3.9)$$

$$\phi_{\omega_2}(k_1) = \phi_{\omega_3}(k_1) = \frac{1}{2}\left(\phi_{\omega_1} - k_1\frac{\partial\phi_{\omega_1}}{\partial k_1}\right) . \quad (3.10)$$

The spectra $\phi_{\omega_i}(k_1)$ can be readily written in terms of ϕ_{u_1} or $\phi_{u_{1,1}}$ (e.g. Van Atta 1991; Kim & Antonia 1993):

$$\phi_{\omega_1}(k_1) = \phi_{u_{1,1}}(k_1) + 4\int_{k_1}^{\infty}\frac{\phi_{u_{1,1}}(k)}{k}\mathrm{d}k \quad (3.11)$$

$$\phi_{\omega_2}(k_1) = \phi_{\omega_3}(k_1) = \tfrac{5}{2}\phi_{u_{1,1}}(k_1) - \frac{k_1}{2}\frac{\partial\phi_{u_{1,1}}(k_1)}{\partial k_1} + 2\int_{k_1}^{\infty}\frac{\phi_{u_{1,1}}(k)}{k}\mathrm{d}k . \quad (3.12)$$

The components of $\phi_{\omega_2}(k_1)$ and $\phi_{\omega_3}(k_1)$ may be written as follows:

$$\phi_{u_{1,2}}(k_1) = \phi_{u_{1,3}}(k_1) = 2\int_{k_1}^{\infty}\frac{1}{k}\phi_{u_{1,1}}(k)\mathrm{d}k, \quad (3.13)$$

$$\phi_{u_{2,1}}(k_1) = \phi_{u_{3,1}}(k_1) = \tfrac{3}{2}\phi_{u_{1,1}}(k_1) - \tfrac{1}{2}k_1\frac{\partial\phi_{u_{1,1}}}{\partial k_1}, \quad (3.14)$$

$$Co_{u_{1,2}u_{2,1}}(k_1) = Co_{u_{1,3}u_{3,1}}(k_1) = -\tfrac{1}{2}\phi_{u_{1,1}}(k_1) . \quad (3.15)$$

Equation (3.15) is obtained by integrating the isotropic form of the cospectrum, namely (2.10) with $\phi_{12}(k)$ given by (2.11), over all values of k_2 and k_3.

4. Experimental details and conditions

Measurements were made in the working section (350 mm × 350 mm, 2.4 m long) of an open return low-turbulence wind tunnel. The bottom wall of the working

U_∞ (m s^{-1})	U_0 (m s^{-1})	d_c (mm)	R_λ	λ (mm)	η (mm)	f_c (kHz)	f_K (kHz)	f_s (kHz)	$\Delta x_3/\eta$	$\Delta x_2/\eta$
3.6	0.35	12.7	60	5.6	0.37	1.6	1.41	3.33	2.43	4.05
5.0	0.58	25	120	6.6	0.32	2.5	2.30	5.0	2.5	4.70
10.0	0.76	25	190	5.1	0.18	8.0	7.7	15.15	4.4	6.1
14.7	1.35	25	260	4.7	0.14	8.0	15.15	15.15	5.7	7.8

TABLE 1. Table 1 Summary of Experimental Conditions at $x_1/d_c = 70$.

section was tilted to achieve a zero streamwise pressure gradient. A definition sketch of the flow and coordinate system is shown in figure 1(*b*). The free-stream velocity U_∞ was varied from 3.6 to 14.7 m s^{-1} and the Reynolds number R_d ($\equiv U_\infty d_c/\nu$, where d_c is the diameter of the cylinder; $d_c = 12.7$ mm for $U_\infty = 3.6$ m s^{-1} and 25 mm for other speeds) was in the range 3000 $\sim$ 24500. Measurements were made in the intermediate wake $x_1/d_c = 70$, where x_1 is the streamwise distance measured from the cylinder axis. Ideally, all measurements should have been made in the self-preserving region of the flow. The present choice ($x_1/d_c = 70$) was a compromise because of the need to use relatively large cylinder diameters to obtain a moderately high R_λ. For the largest diameter used here ($d_c = 25$ mm), the length of the working section precluded the use of distances much greater than $70d_c$.

The mean velocity defect on the wake centreline, denoted by U_0, and centreline values of the Kolmogorov length scale η ($\equiv \nu^{3/4}/\bar{\epsilon}^{1/4}$), where $\bar{\epsilon}$ was estimated by assuming isotropy, namely $\bar{\epsilon} = 15\nu\overline{u_{1,1}^2}$ are given in table 1. Centreline values of λ (Taylor's hypothesis $u_{1,1} = -\overline{U}_1^{-1}u_{1,t}$ was used) and the associated values of the turbulence Reynolds number R_λ are also given in table 1. The use of isotropic values $\bar{\epsilon}$ results in only small errors in η. The data of Browne, Antonia & Shah (1987) suggest that $\bar{\epsilon}_{iso}/\bar{\epsilon}$ is about 0.90 on the wake centreline; the resulting maximum error in η would be of order 1 or 2%.

When the present probe measured ω_3 (figure 1*a*) two parallel wires were aligned in the x_3-direction but separated in the x_2-direction and the X-wire was in the (x_1, x_2)-plane. The separations Δx_2^* and Δx_3^* were adjusted (table 1) at each Reynolds number in order to (i) minimize the attenuation due to too large a separation and (ii) avoid noise contamination and the possibility of probe interference due to too small a separation. For the choice of the separation Δx_2^*, we relied mainly on a separate experiment in which the separation between two single hot wires, parallel to the x_3-direction, was varied in the range 0.2 mm to 5 mm. This variation allowed estimates of $\overline{u_{1,2}^2}^{1/2}$ by the finite difference technique (Antonia *et al.* 1984; Antonia & Mi 1993*a*; Zhu *et al.* 1993) and the correlation method (Taylor 1935; Rose 1966; Verollet 1972; Browne *et al.* 1987). The separation Δx_3^* was greater than 2 (at each Reynolds number); this choice is consistent with the suggestion in Zhu & Antonia (1995*b*). For the measurement of ω_2, the probe was rotated through 90° so that the X-wires were in the (x_1, x_3) plane. 2.5 μm diameter Wollaston (Pt–10% Rh) hot wires were used for the probe. The wires were etched to a length of about 0.5 mm.

Thin prongs (the tip diameter was about 0.1 mm) were used to minimize the flow blockage. The included angle for X-wires was about 100° in order to minimize any adverse effects associated with large velocity-vector cone angles (e.g. Perry, Lim & Henbest 1987; Browne, Antonia & Chua 1989). No correction to the X-wires was made for the possible effect of $\overline{U}_{1,2}$ since this mean velocity gradient is zero on

the centreline. Taylor's hypothesis is approximately satisfied (Mi & Antonia 1996); therefore, corrections for the influence of a fluctuating velocity field were not made. In order to minimize the effect of wind-tunnel induced vibration, the hot-wire probes were mounted in isolation from the tunnel.

The hot wires were operated with in-house constant-temperature circuits at an overheat ratio of 0.5. Output voltages from the anemometers were passed through buck and gain circuits and low-pass filtered at a cut-off frequency f_c, typically in the range 1.6 to 8 kHz. A few comments should be made on the choice of f_c since vorticity is a small-scale characteristic. The selection of f_c is by necessity a compromise between the need to use as high a value as possible while minimizing the effect of noise. Too high a filter setting would result in the signal being contaminated by an excessive amount of electronic noise while too low a setting would cause the high-frequency part of the spectrum to be attenuated. In this experiment, the procedure used to select f_c was essentially that outlined in Antonia, Satyaprakash & Hussain (1982). All four anemometer signals were first differentiated using analogue circuits and the spectra of the differentiator output signals were viewed on the screen of a real time spectrum analyser (HP3582A). It was relatively easy to identify a frequency, f_{min} say, in the relatively high-frequency part of the spectrum where the spectral density started to level off before increasing at higher frequencies. This behaviour was associated with the contamination due to noise since the outputs from the differentiators exhibited a similar trend when the hot wires were disconnected and the inputs to the constant-temperature circuits were shorted. Since one would expect some noise contamination for frequencies smaller than f_{min}, f_c ($< f_{min}$) was selected where the spectral density was 2–3 dB higher than that at f_{min}.

For $U_\infty = 3.6$ m s^{-1} and $U_\infty = 5$ m s^{-1}, f_c (table 1) was equal to 1.6 kHz and 2.5 kHz respectively. These values are about 13% and 9% higher than the values of $f_K \equiv \overline{U}_1/2\pi\eta$ (table 1). For $U_\infty = 10$ m s^{-1}, f_c was slightly larger than f_K. For $U_\infty = 14.7$ m s^{-1}, f_c was equal to 8 kHz. This choice was dictated by the maximum sampling frequency of the data acquisition board which was about 16 kHz per channel (when four channels are used). Although data were recorded for $U_\infty = 14.7$ m s^{-1}, the records were used only to examine inertial-range statistics; dissipation-range statistics, which would have been affected by the failure to resolve the high-frequency content up to f_K, have not been included in §§5 and 6.

The choice $f_c \simeq f_K$ is consistent with the suggestions of Kuo & Corrsin (1971), Frenkiel & Klebanoff (1975), Champagne (1978) and Frenkiel, Klebanoff & Huang (1979) in connection with the measurement of small-scale statistics. Antonia *et al.* (1982) found that the use of $f_c \simeq f_K$ underestimated $S_{u_{1,1}}$ and $F_{u_{1,1}}$ by about 10% compared to the values obtained when $f_c \simeq 1.75 f_K$ while Browne *et al.* (1987) reported that their measured values of $S_{u_{1,1}}$ and $F_{u_{1,1}}$ were approximately constant for $f_c \geqslant f_K$. In order to examine the appropriateness of the present choice of f_c, we measured F_α ($\alpha = u_{1,1}$, $u_{1,2}$, $u_{2,1}$ and ω_3) using a value of f_c which is 12% smaller than that listed in table 1 for $U_1 = 10$ m s^{-1}. The measured values were within 5% of those obtained using $f_c = 8$ kHz, indicating that the selection of $f_c \simeq f_K$ should be satisfactory for the present investigation.

The filtered signals were sampled at $f_s \approx 2f_c$ (table 1) into a personal computer (NEC 386) using a 12-bit A/D converter (RC Electronics). Record durations of about 2 min were used. Yaw and velocity calibrations were carried out on the PC but all other processing of the data was done on a VAX 8550 computer.

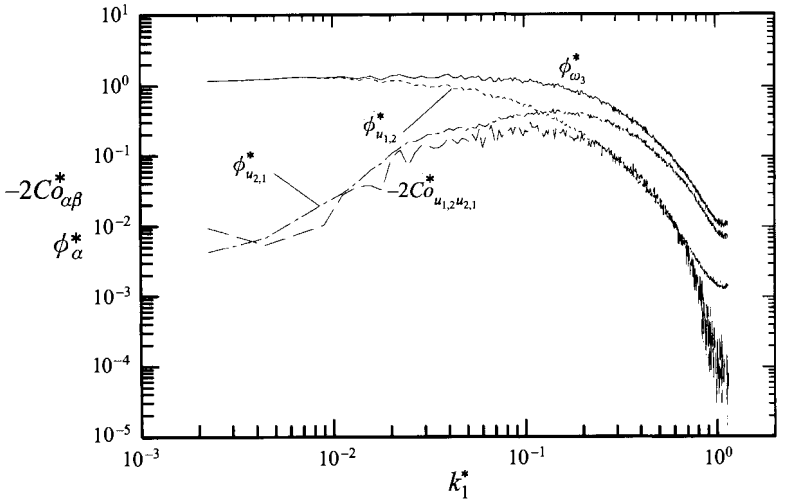

FIGURE 3. Measured (uncorrected) spectra of ω_3 and of its components ($R_\lambda = 60$).

5. Measured vorticity spectra and spectral checks of local isotropy

We underlined in §2 that the correction to the vorticity spectrum does not hinge critically on the assumption of isotropy. Figure 3 shows the contributions to ϕ_{ω_3} from the three constituents of ω_3. The spectra are shown up to the data acquisition frequency. The slight upturning of the spectra around $k_1^* \simeq 1.0$ is due to the electronic noise. The largest contribution is made by $\phi_{u_{2,1}}$ at $k_1^* \simeq 0.22$; the peak values of $\phi_{u_{1,2}}$ and $-2Co_{u_{1,2}u_{1,2}}$ occur at smaller values of k_1^*. Whereas $\phi_{u_{1,2}}$ is more dominant at lower wavenumbers ($k_1^* \lesssim 0.1$), $\phi_{u_{2,1}}$ dominates at high wavenumbers ($k_1^* \gtrsim 0.2$), almost one decade larger than the other two components. When integrated over all values of k_1^*, $\phi_{u_{1,2}}$ and $\phi_{u_{2,1}}$ make approximately equal contributions (39% and 41%) to $\overline{\omega_3^2}$. Although the spectra shown in figure 3 are uncorrected, the conclusions drawn here also apply to the corrected spectra.

There are a number of tests for checking whether the high-wavenumber part of the spectrum conforms with isotropy. For example, the u_1u_2 cospectrum should be zero; figure 4 indicates that this is the case when $k_1^* \gtrsim 0.08$ for $R_\lambda = 60$ and $k_1^* \gtrsim 0.02$ for $R_\lambda = 190$. The measured u_2 spectrum in figure 5 compares favourably with the calculation based on the measured u_1 spectrum from the single hot wire via (3.9). The agreement is always better than 20% in the range $k_1^* \gtrsim 0.08$. The anisotropy is apparent at lower wavenumbers. The mild peak at $k_1^* \simeq 0.02$ is not associated with the vortex shedding; it reflects the onset of the organized large-scale motion ($k_1^* = 0.02$ corresponds to a ratio L_c/λ_c of about 0.23, which is the value previously established by Antonia, Browne & Fulachier 1987; L_c is the wake half-width and λ_c is the average streamwise wavelength of the large-scale motion) in the far wake. The u_3 spectrum, also shown in figure 5, is indistinguishable from the u_2 spectrum, at least in the range $k_1^* \gtrsim 0.05$. While this equality is consistent with local isotropy, namely (3.9), it is arguably not a stringent requirement since the assumption of axisymmetry would also require that ϕ_{u_2} and ϕ_{u_3} are equal, with x_1 being the preferred direction. In this context, one would also expect ϕ_{ω_2} and ϕ_{ω_3} to be equal, as will be shown later in this section.

In testing hypotheses for the small-scale structure of turbulence, it is important to select quantities which are representative of the small-scale motion (Antonia & Kim

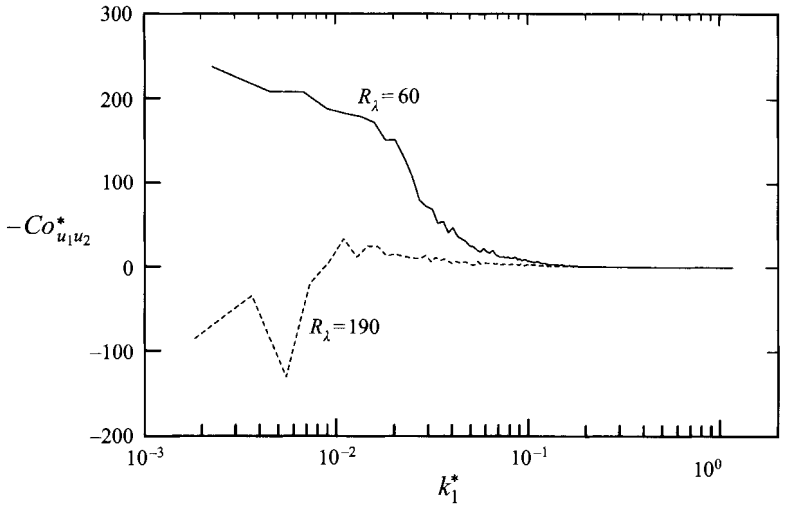

FIGURE 4. Measured u_1u_2 cospectrum.

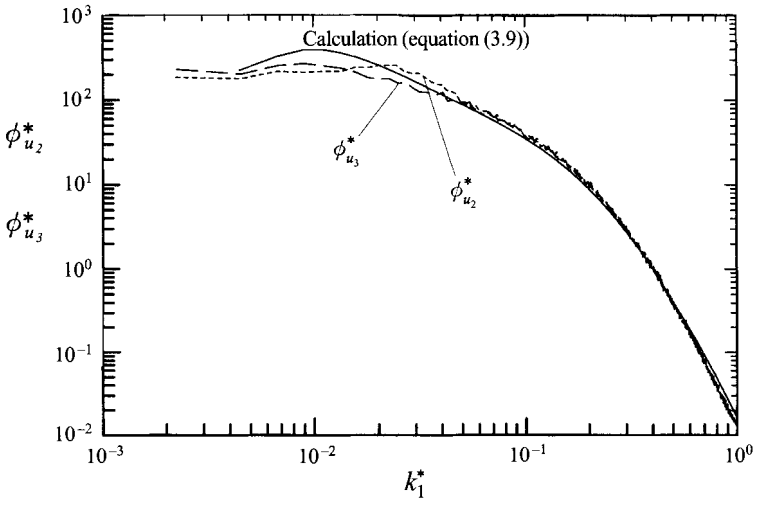

FIGURE 5. Measured u_2, u_3 spectra and comparison with isotropy ($R_\lambda = 60$).

1994). Here we use the corrected spectra of ω_i ($i = 2,3$) and $u_{i,j}$ to test local isotropy. The spectra of ω_i and its components are compared with isotropic calculations in figures 6 and 7. The present corrected spectra of ω_i agree with corrected spectra (not shown here) obtained with a two-X-wire probe in the same flow ($x_1/d_c = 70$, $R_\lambda = 60$); this further supports the claim made in §2 with regard to the validity of the correction procedure. The calculations were done using (3.12)–(3.15) and the measured $u_{1,1}$ spectrum ($\phi_{u_{1,1}}$ was determined by first differentiating the time series of u_1; this procedure results in a better signal-to-noise ratio for $\phi_{u_{1,1}}$ than if the latter quantity is formed by multiplying ϕ_{u_1} with k_1^2). Figure 6 indicates that $\phi_{u_{2,1}}$ and $\phi_{u_{3,1}}$ are almost identical and agree well with calculation (equation (3.14)) when $k_1^* \gtrsim 0.2$. $Co_{u_{1,3}u_{3,1}}$ and $Co_{u_{1,2}u_{2,1}}$ also agree with the calculation (equation (3.15)) when $0.02 \leqslant k_1^* \leqslant 0.4$. However, for $k_1^* \gtrsim 0.4$, they fall below the calculation.

$\phi_{u_{1,2}}$ and $\phi_{u_{1,3}}$ (figure 7) are also identical and follow the calculation closely even

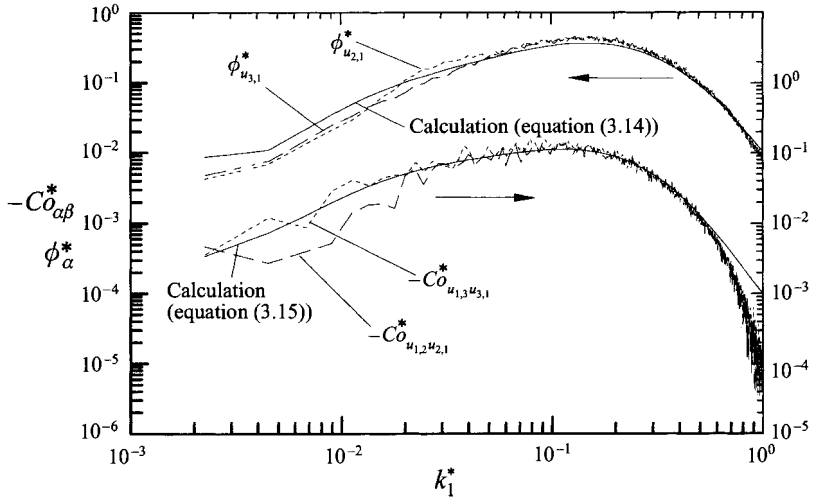

FIGURE 6. Corrected spectra of vorticity components and comparison with isotropy ($R_\lambda = 60$).

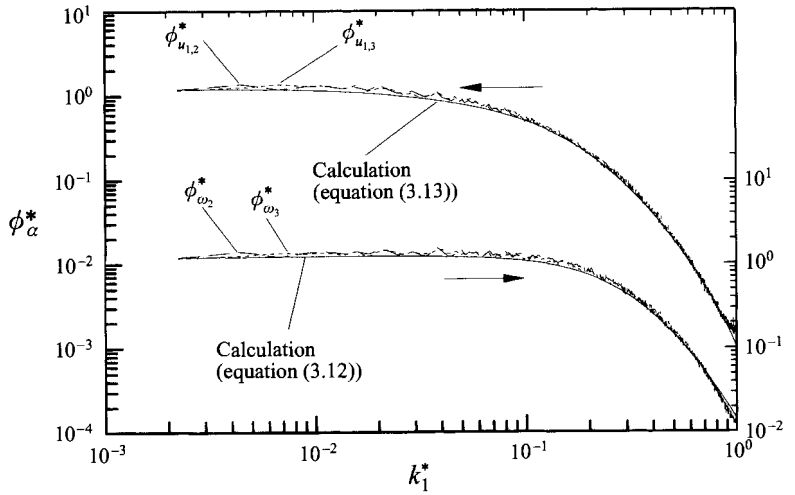

FIGURE 7. Corrected spectra of vorticity and its components and comparison with isotropy ($R_\lambda = 60$).

at low wavenumbers. Since the spectra of the components of ω_2 and ω_3 are (nearly) identical, ϕ_{ω_2} and ϕ_{ω_3} should also be the same. This is indeed the case: figure 7 shows that ϕ_{ω_2} and ϕ_{ω_3} are practically indistinguishable from each other and in satisfactory agreement with the isotropic calculations via (3.12).

The results presented in this section were obtained at $R_\lambda = 60$, too small for an inertial range to exist and, arguably, for local isotropy to be valid. Yet, most of the statistics presented seem to conform closely with isotropy. This trend is consistent with Antonia & Kim's (1994) conclusion, based on direct numerical simulations of various turbulent flows, that isotropy is satisfied independently of the quantity considered or R_λ provided k_1^* is sufficiently large and the Kolmogorov-normalized mean strain rate is sufficiently small. The isotropic checks (not shown here) for higher R_λ indicate that the level of agreement with local isotropy is about the same as for low-R_λ data; the range of agreement, however, extends to lower wavenumbers as R_λ increases.

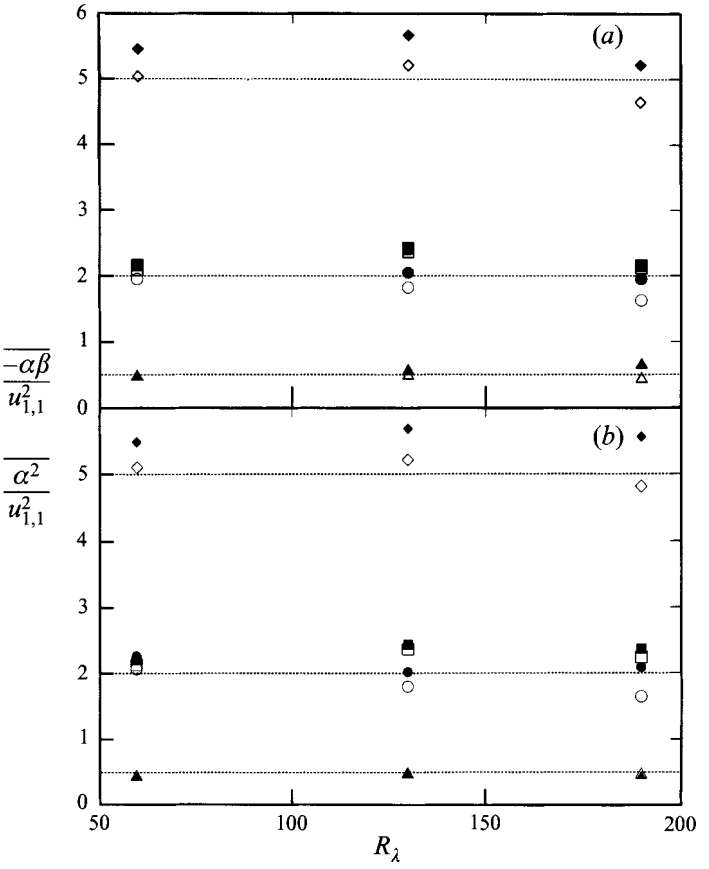

FIGURE 8. Ratio of $\overline{\omega_i^2}$ and its components to $\overline{u_{1,1}^2}$. Open symbols: uncorrected. Closed symbols: corrected. Dotted lines: isotropic values. (*a*) ◆, ◇ , $\overline{\omega_2^2}/\overline{u_{1,1}^2}$; ■, □, $\overline{u_{3,1}^2}/\overline{u_{1,1}^2}$; ●, ○, $\overline{u_{1,3}^2}/\overline{u_{1,1}^2}$; ▲, △, $-\overline{u_{1,3}u_{3,1}}/\overline{u_{1,1}^2}$. (*b*) ◆, ◇, $\overline{\omega_3^2}/\overline{u_{1,1}^2}$; ■, □, $\overline{u_{2,1}^2}/\overline{u_{1,1}^2}$; ●, ○, $\overline{u_{1,2}^2}/\overline{u_{1,1}^2}$; ▲, △, $-\overline{u_{1,2}u_{2,1}}/\overline{u_{1,1}^2}$.

6. Dependence on R_λ

Statistics of $u_{1,1}$ and their dependence on R_λ have been of interest in the context of small-scale intermittency (e.g. Van Atta & Antonia 1980). Assuming $\tilde{\epsilon} \sim u_{1,1}^2$ to be an appropriate replacement for ϵ, statistical properties of ϵ have been inferred from those of $\tilde{\epsilon}$. Since vorticity is closely connected with fine-scale turbulence, it seems appropriate to investigate the R_λ dependence of the statistics of ω_i.

Figure 8 shows the ratios of $\overline{\omega_2^2}$, $\overline{\omega_3^2}$ and their components to $\overline{u_{1,1}^2}$ for three values of R_λ (60, 120 and 190). While the measured ratio $\overline{\omega_i^2}/\overline{u_{1,1}^2}$ is close to the isotropic value of 5, equation (3.1), the corrected ratio is greater than the isotropic value. The maximum deviation ($R_\lambda = 120$) is about 12%. This discrepancy appears to be associated with the deviation ($\simeq$ 20%) of $\overline{u_{2,1}^2}/\overline{u_{1,1}^2}$ and $\overline{u_{3,1}^2}/\overline{u_{1,1}^2}$ from the isotropic value of 2 (equation (3.3)). The other quantities agree with isotropy to within $\pm$6%. Note that these ratios are determined with relatively high accuracy since the correction that needs to be applied to $\overline{u_{1,1}^2}$, $\overline{u_{2,1}^2}$ and $\overline{u_{3,1}^2}$ is small and does not depend on local isotropy. Also, estimates of these three variances obtained from the correlation method agreed to $\pm$1% with those estimated from the finite difference

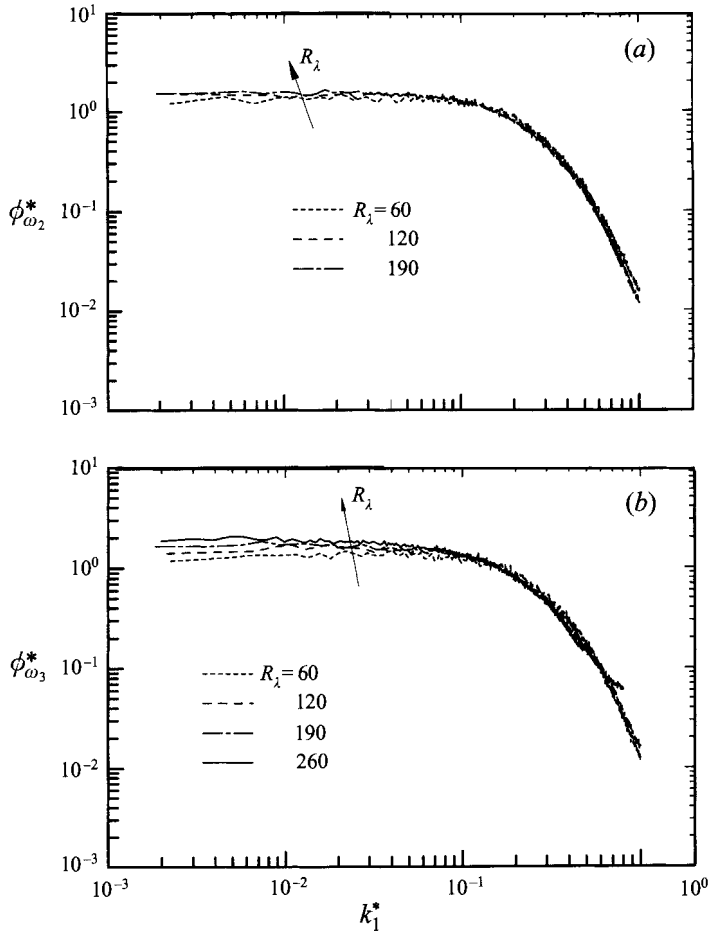

FIGURE 9. Corrected spectra of ω_2 and ω_3.

method. Figure 8 indicates that local isotropy is only approximately satisfied. The slight departure from isotropy is arguably due to the fact that the measurements were made just beyond the intermediate region of the wake where the near-wake organized (and anisotropic) large-scale motion may still be exerting an influence on the statistics. In this context, the variances of vorticity and its components, which weight all wavenumbers, may not be a good indicator of the isotropy of the fine structure.

According to figure 9, both $\phi^*_{\omega_2}$ and $\phi^*_{\omega_3}$ show a reasonable collapse at high wavenumbers for different R_λ. The collapse appears to be consistent with Kolmogorov's similarity hypothesis (Kolmogorov, 1941). At low wavenumbers, however, the magnitudes of $\phi^*_{\omega_2}$ and, more especially, $\phi^*_{\omega_3}$ increase slightly with R_λ. This behaviour is not surprising in that there is no *a priori* reason why Kolmogorov scaling should be appropriate at low wavenumbers. The integrals under the spectra in figure 9 yield $\overline{\omega_2^{*2}}$ or $\overline{\omega_3^{*2}}$. The magnitudes of these two quantities increase only marginally with R_λ: in the case of $\overline{\omega_3^{*2}}$, the increase is from 0.38 at $R_\lambda = 60$ to 0.39 at $R_\lambda = 190$. Note that for homogeneous turbulence $\bar{\epsilon} = \nu\overline{\omega^2}$, so that $\overline{\omega^{*2}} = 1$. With the additional assumption of isotropy, $\overline{\omega_1^{*2}} = \overline{\omega_2^{*2}} = \overline{\omega_3^{*2}} = 1/3$. The present values of $\overline{\omega_2^{*2}}$ and $\overline{\omega_3^{*2}}$

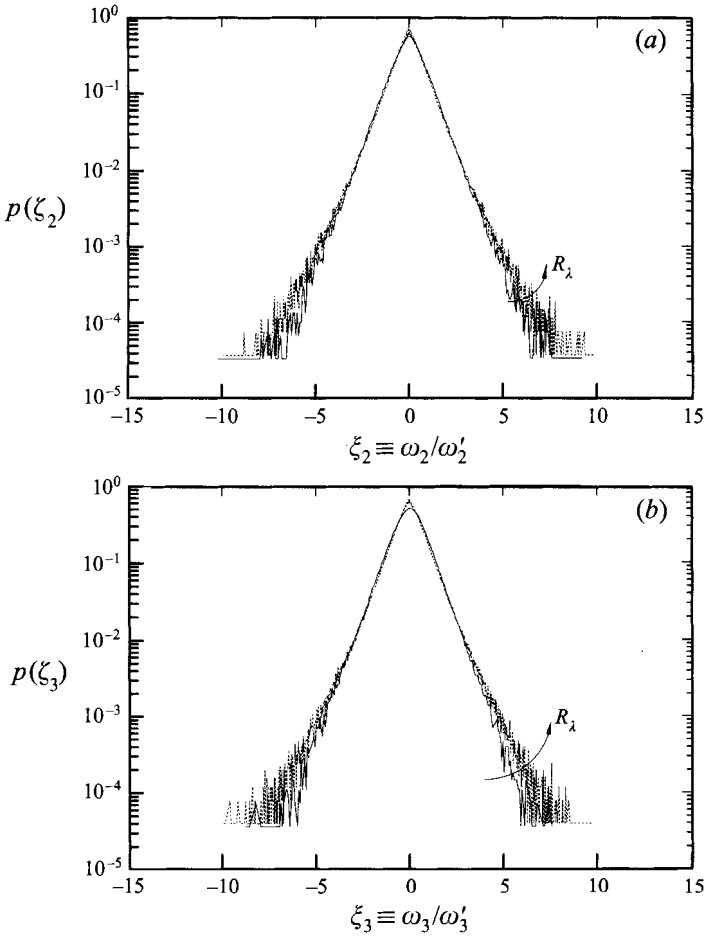

FIGURE 10. Probability density functions of ω_2 and ω_3. Prime denotes r.m.s. of the quantity. (*a*) ω_2: —, $R_\lambda = 60$; ·, 190. (*b*) ω_3: —, $R_\lambda = 60$; ·, 190.

are somewhat larger than 1/3, possibly reflecting small departures from homogeneity and isotropy at $x_1/d_c = 70$. It should also be recalled that the isotropic value of $\bar{\epsilon}$ has been used for normalization: the use of the total dissipation (which is greater than $\bar{\epsilon}_{iso}$) would result in a reduction of the present values of $\overline{\omega_2^{*2}}$ and $\overline{\omega_3^{*2}}$. A comment on the scaling of $\overline{\omega^2}$ in the self-preserving far wake seems appropriate here. In this region of the flow, one expects $\bar{\epsilon}$ to scale on L_c and U_0, i.e. $\bar{\epsilon}L_c/U_0^3 = f(y/L_c)$ or, provided homogeneity is a reasonable approximation, $\overline{\omega^2}L_c^2/U_0^2 = R_\lambda f(y/L_c)$. The vorticity variance should therefore increase linearly with R_λ, when normalized by the characteristic wake scales. Data collected by Mi & Antonia (1994) for the far wake support this result.

The dependence on R_λ can also be quantified through the probability density function of ω and its components. Figures 10(*a*) and 10(*b*) plot the p.d.f.s of ω_2 and ω_3, respectively. At $R_\lambda = 60$, the p.d.f.s assume a nearly exponential form. For small ζ_i ($\equiv \omega_i/\omega_i'$), there is little difference in the p.d.f.s for different R_λ. For large ζ_i, however, evolve with R_λ, a double exponential behaviour becoming more evident as R_λ increases. Note that we do not know how to correct $p(\zeta_i)$ for the effect of spatial resolution.

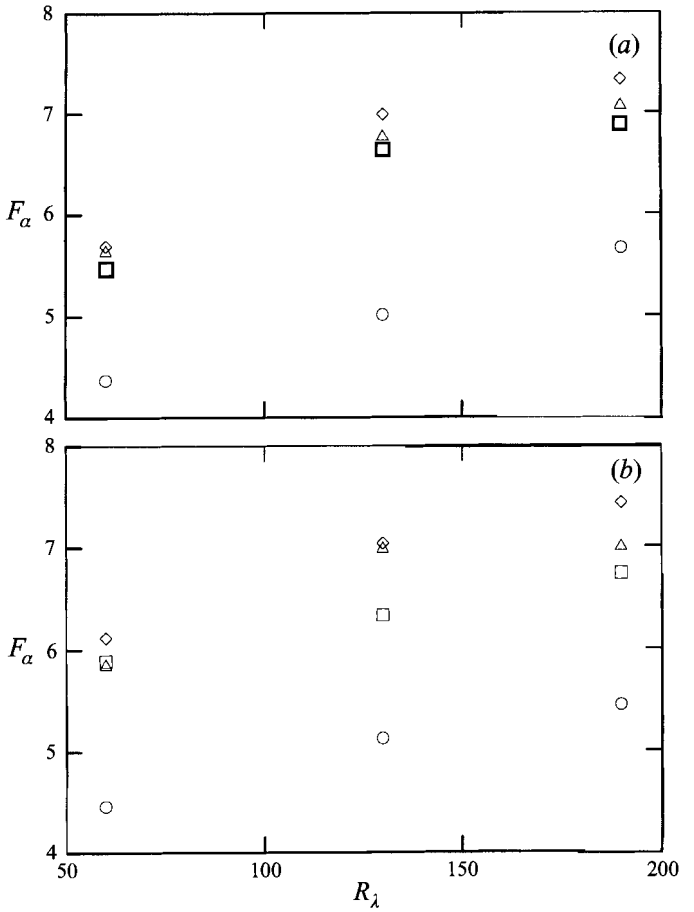

FIGURE 11. Flatness factors of ω_2, ω_3 and their components. (*a*) ω_2 : ○, $u_{1,1}$; □, $u_{3,1}$; △, $u_{1,3}$; ◇, ω_2. (*b*) ω_3 : ○, $u_{1,1}$; □, $u_{2,1}$; △, $u_{1,2}$; ◇, ω_3.

At $x_1/d_c = 70$, $p(\zeta_2)$ and $p(\zeta_3)$ are virtually identical, irrespective of R_λ. This is consistent with the previously noted equality (equation (3.1)) between second-order moments of ω_2 and ω_3. The approximate symmetry of these p.d.f.s about the origin implies that all odd-order moments should be very close to zero. Indeed, all the skewnesses (not shown) for the two components of vorticity are nearly zero. However, a zero skewness does not necessarily validate local isotropy since the flow is symmetrical about the centreline. The flatness factors of ω_2 and ω_3, i.e. F_{ω_2} and F_{ω_3}, are nearly the same (figure 11). Figure 11 also indicates that the flatness factor of vorticity and its components increases with R_λ, which is consistent with the previously observed behaviour of $p(\zeta_2)$ and $p(\zeta_3)$. The magnitudes of F_{ω_2} and F_{ω_3} are slightly higher than the flatness factors of the components of ω_2 and ω_3 but noticeably larger than the magnitude of $F_{u_{1,1}}$. One could associate, albeit with some qualifications, the flatness factors of $u_{i,j}$ or ω_i with intermittency (e.g. Sreenivasan 1995). Correspondingly, figure 11 implies that vorticity becomes more intermittent as R_λ increases. It also shows that $u_{1,1}$ is the least intermittent of the quantities, so that intermittency characteristics inferred from $u_{1,1}$ are unlikely to apply exactly to other components of $u_{i,j}$ or vorticity. Since, for homogeneous and isotropic turbulence,

$\bar{\epsilon} = 3\nu\overline{\omega_3^2}$, the flatness factors of ω_i ($i = 2,3$) may be more representative of the dissipation field than those of $u_{1,1}$. The difference between the magnitudes of F_{ω_2} (or F_{ω_3}) and $F_{u_{1,1}}$ is significant and represents an appreciable departure from the isotropic relation (3.7). Note that the magnitudes of $F_{u_{2,1}}$ and $F_{u_{3,1}}$ are also greater than $F_{u_{1,1}}$, which contravenes relation (3.8). The departures from isotropy indicated by figure 11 reflect the anisotropy of both fourth-order and second-order moments; we emphasize that these moments weight the anisotropy of the larger scales of motion so that the results of figure 11 do not negate previous conclusions regarding the approximate isotropy at high wavenumbers. It should also be noted that, whereas corrected second-order moments of ω_i are attainable via the corrected spectrum, we do not know how to correct moments of order greater than 2. The reliability of $\overline{\omega_i^4}$ or, more generally, $p(\omega_i)$ cannot therefore be guaranteed. However, if one normalizes the fourth-order moments by the corrected second-order moments, some compensation can be expected. The statistical convergence of $\overline{\omega_i^4}$ was verified for the present measurements since the product $\overline{\omega_i^4} p(\omega_i)$ was negligible at sufficiently large values of $|\omega_i|$.

7. Inertial-range behaviour

For homogeneous turbulence, the vorticity correlation tensor $B_{ij}^{\omega}(\boldsymbol{r}) = \overline{\omega_i(\boldsymbol{x})\omega_j(\boldsymbol{x}+\boldsymbol{r})}$ is related to the velocity correlation tensor $B_{ij}(\boldsymbol{r}) \equiv \overline{u_i(\boldsymbol{x})u_j(\boldsymbol{x}+\boldsymbol{r})}$ through the Navier–Stokes equations (Batchelor 1953; Monin & Yaglom 1975)

$$B_{ij}^{\omega} = -\delta_{ij}\frac{\partial^2 B_{kk}}{\partial r_i \partial r_i} + \frac{\partial^2 B_{kk}}{\partial r_i \partial r_j} + \frac{\partial^2 B_{ij}}{\partial r_i \partial r_i}\,. \tag{7.1}$$

For isotropic turbulence, the dependence on the separation vector $\boldsymbol{r}$ may be replaced by a dependence on the scalar r (the magnitude of $\boldsymbol{r}$). In this case, $B_{ij}^{\omega}(r)$ and $B_{ij}(r)$ are given by

$$B_{ij}^{\omega}(r) = \left(B_{LL}^{\omega} - B_{NN}^{\omega}\right)\frac{r_i r_j}{r^2} + B_{NN}^{\omega}\delta_{ij} \tag{7.2}$$

and

$$B_{ij}(r) = (B_{LL} - B_{NN})\frac{r_i r_j}{r^2} + B_{NN}\delta_{ij} \tag{7.3}$$

respectively, where the subscripts LL and NN refer to the longitudinal and lateral correlations respectively (the notation follows essentially that used in Monin & Yaglom). If f and g are the scalar longitudinal and lateral correlation functions, $f \equiv B_{11}$, $g \equiv B_{22}$ or B_{33}, $f^{\omega} = B_{11}^{\omega}$, $g^{\omega} = B_{22}^{\omega}$ or B_{33}^{ω}. As noted in §3, vorticity and velocity are both solenoidal, i.e. $\partial B_{ij}^{\omega}/\partial r_j = 0$ and $\partial B_{ij}/\partial r_j = 0$. It follows that $g^{\omega} = f^{\omega} + (r/2)f^{\omega'}$ and $g = f + (r/2)f'$, the prime denoting differentiation with respect to r. Expressions for f^{ω} and g^{ω} can be obtained after substituting (7.3) into (7.1) (note that $B_{kk} = f + 2g$):

$$f^{\omega} = f'' - 4\frac{g'}{r} - 4\frac{f-g}{r^2}, \tag{7.4}$$

$$g^{\omega} = -f'' - g'' - \frac{f'}{r} + 2\frac{f-g}{r^2}\,. \tag{7.5}$$

In the inertial range ($\eta \ll r \ll L$; L is the integral length scale), the behaviours of f and g follow from the '$r^{2/3}$' dependence of the velocity structure functions

(Kolmogorov 1941), i.e.

$$f = f(0) - \tfrac{1}{2}C\bar{\epsilon}^{2/3}r^{2/3}, \tag{7.6}$$

$$g = g(0) - \tfrac{2}{3}C\bar{\epsilon}^{2/3}r^{2/3}, \tag{7.7}$$

where $f(0)$, which is equal to $g(0)$, is the correlation at zero separation and C is the Kolmogorov constant. Substitution of (7.6) and (7.7) into (7.4) and (7.5) yields a $r^{-4/3}$ dependence for f^{ω} and g^{ω}:

$$f^{\omega} = \tfrac{11}{9}C\bar{\epsilon}^{2/3}r^{-4/3}, \tag{7.8}$$

$$g^{\omega} = \tfrac{11}{27}C\bar{\epsilon}^{2/3}r^{-4/3}. \tag{7.9}$$

Whereas (7.8) and (7.9) indicate that inertial-range power-law distributions should be observed in vorticity correlations, (7.6) and (7.7) suggest that a power-law behaviour should be seen only on the differences $f(0)-f$ or $f(0)-g$ rather than directly on f or g. Given that vorticity correlations are associated with small-scale motion, the condition of isotropy can be relaxed to that of local isotropy. To our knowledge, there have been no previous attempts to verify (7.8) or (7.9). A $r^{-4/3}$ inertial-range behaviour for $\overline{(\Delta\omega)^2}$, the second-order vorticity structure function, can be derived using dimensional arguments similar to those used by Kolmogorov (1941) in obtaining a $r^{2/3}$ inertial-range dependence for $\overline{(\Delta u)^2}$. Assuming that the vorticity increment $\Delta\omega$ depends on r and $\bar{\epsilon}$ in the inertial range, it can be shown that $\overline{(\Delta\omega)^2} \sim \bar{\epsilon}^{2/3}r^{-4/3}$ or, alternatively, $\overline{(\Delta\omega^*)^2} \sim r^{*-4/3}$. Note however that this argument is erroneous since it leads to a $r^{-4/3}$ behaviour for the second-order structure function and not the correlation; the present experimental data (see below) support a $r^{-4/3}$ behaviour for the correlation only.

The present data for the lateral correlation coefficient $\rho_{\omega_3} \equiv \overline{\omega_3(x_1)\omega_3(x_1+r)}/\overline{\omega_3^2}$ are shown in figure 12 for $R_\lambda = 260$. This Reynolds number is sufficiently large for an inertial range to be observed in the second-order velocity structure function $\overline{(\Delta u_1)^2} \equiv \overline{[u_1(x_1+r)-u_1(x)]^2}$. Although the sampling frequency is low compared with the Kolmogorov frequency, it should be appropriate for the present purpose. The values of $r^{*-2/3}\overline{(\Delta u_1^*)^2}$, also shown in figure 12, are approximately constant over the range $30 \lesssim r^* \lesssim 200$; the plateau implies a value of C of about 2, in reasonable agreement with the bulk of laboratory and atmospheric data for this constant (Yaglom 1981). In the inertial range, the agreement with (7.9) is reasonable. It should be noted that the ρ_{ω_3} data in figure 12 have been corrected for the effect of spatial averaging since they were obtained by inverse Fourier transforming the corrected ω_3 spectrum (however, the magnitude of the correction is small in the inertial range). The large scatter in the inertial-range data for ρ_{ω_3} reflects the large uncertainty associated with the small magnitudes of the correlation.

8. Comparison with other data

It is of interest to compare the present vorticity statistics with those obtained in other flows. This comparison is important in terms of both further justifying the present data and exploring the R_λ dependence of vorticity statistics.

Figure 13 compares the present $p(\zeta_2)$ and $p(\zeta_3)$ distributions at $R_\lambda = 120$ with $p(\zeta_1)$ obtained from a direct numerical simulation of fully developed turbulence by Kida & Murakami (1989) at $R_\lambda = 128$. The distributions are in good agreement for values of ζ_i around zero. The present distributions tend however to spread to larger values of ζ_i than for Kida & Murakami. The latter distribution is closely approximated by

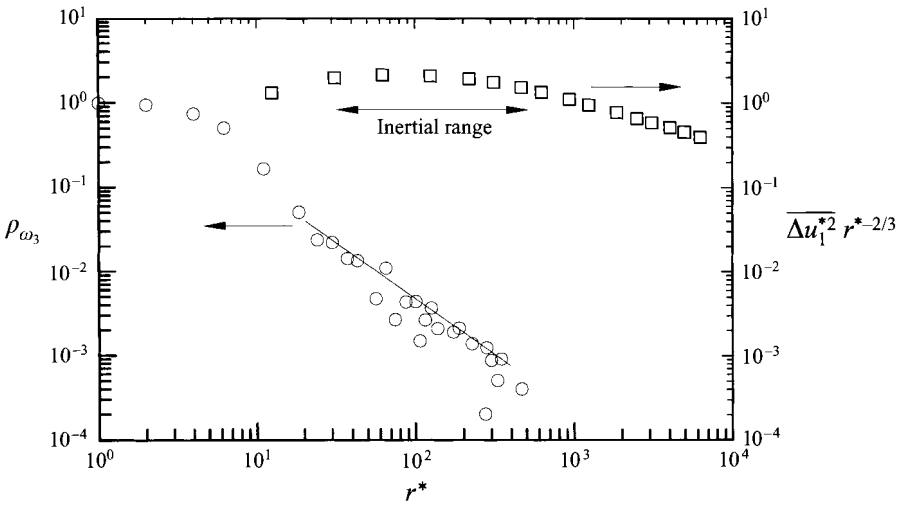

FIGURE 12. Dependence of vorticity correlation coefficient and second-order velocity structure function on r^*. ○, ρ_{ω_3}; □, $\overline{\Delta u_1^{*2}} r^{*-2/3}$; —, equation (7.9).

a single exponential curve (as noted earlier, this is observed in the present data for $R_\lambda = 60$) whereas the present distributions exhibit a double exponential behaviour. Figure 14 indicates that the distribution of $p(\zeta_1)$ measured by Fan (1991) in the wake of a circular cylinder at $R_\lambda = 300$ differs significantly from the present distributions of $p(\zeta_3)$ at $R_\lambda = 260$. Fan's data follow a Gaussian distribution over a central range $|\zeta_1| \lesssim 2.5$ and an exponential distribution for larger $|\zeta_1|$. Fan's grid turbulence measurements of $p(\zeta_1)$ ($R_\lambda = 50$) are similar to those he obtained in the wake, but his atmospheric data for $p(\zeta_1)$, obtained with the same probe, have the same shape as the present distributions of $p(\zeta_3)$. It is unlikely that the difference between $p(\zeta_1)$ and $p(\zeta_2)$ or $p(\zeta_3)$ in figure 14 reflects a genuine difference between ζ_1 and the other two vorticity components. For isotropic turbulence, one would expect that $p(\zeta_1) = p(\zeta_2) = p(\zeta_3)$; recall that the skewness should be zero while the even-order moments of ω_i considered in §3 are independent of i. It should also be noted that distributions of $p(u_{1,1})$ and $p(u_{1,2})$ tend to have an exponential appearance (e.g. Jimenez *et al.* 1993). Accordingly, one would expect $p(\zeta_i)$ to exhibit an exponential behaviour since both $u_{i,j}$ and ω_i are representative of the small scales. In this sense, the behaviour of $p(\zeta_1)$ in figure 14 appears to be inconsistent with the expectation. The difference between Fan's wake data for $p(\zeta_1)$ and the present data for $p(\zeta_2)$ or $p(\zeta_3)$ needs to be investigated further.

The vorticity flatness factor F_{ω_i} is plotted as a function of R_λ in figure 15. The present data appear to extend the trend suggested by the DNS data of Kerr (1985), i.e. F_{ω_i} increases with R_λ in a manner similar to the increase of $F_{u_{1,1}}$ (the solid line represents a least-squares fit to the data of Van Atta & Antonia 1980). It is difficult to comment on the relative rates of increase with R_λ of F_{ω_i} and $F_{u_{1,1}}$, partly because of the lack of F_{ω_i} data at high values of R_λ (the atmospheric point of Fan, for $R_\lambda = 2000$, is probably questionable in view of the earlier comments; this would also apply to the other two measurements by Fan) and also because of the increasing uncertainty in the value of F_{ω_i} when R_λ increases. While there does not yet seem to be a procedure for correcting fourth (or higher)-order moments, it is in principle possible to experimentally determine the effect of spatial resolution on F_{ω_i}, but the implementation could be laborious and increasingly difficult with increasing R_λ. On

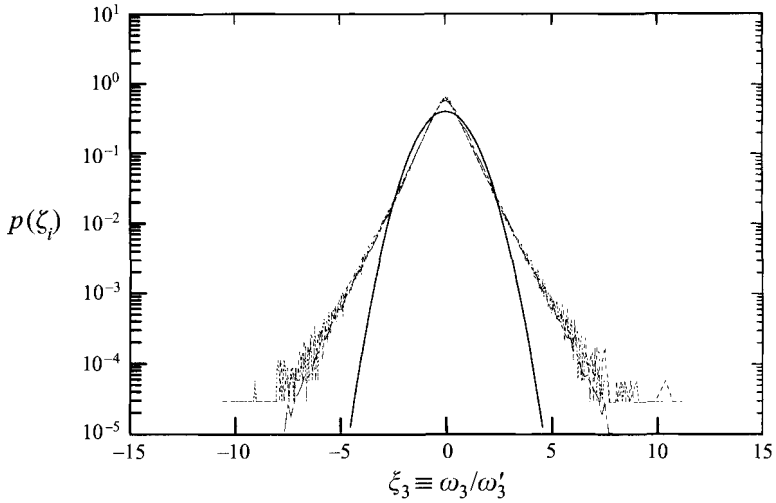

FIGURE 13. Probability density function of ω_i. – - –, $i = 1$, Kida & Murakami (1989), $R_\lambda = 128$; ···, $i = 2$, present, $R_\lambda = 120$; - - -, $i = 3$, present, $R_\lambda = 120$; —, Gaussian distribution with a variance of 1.

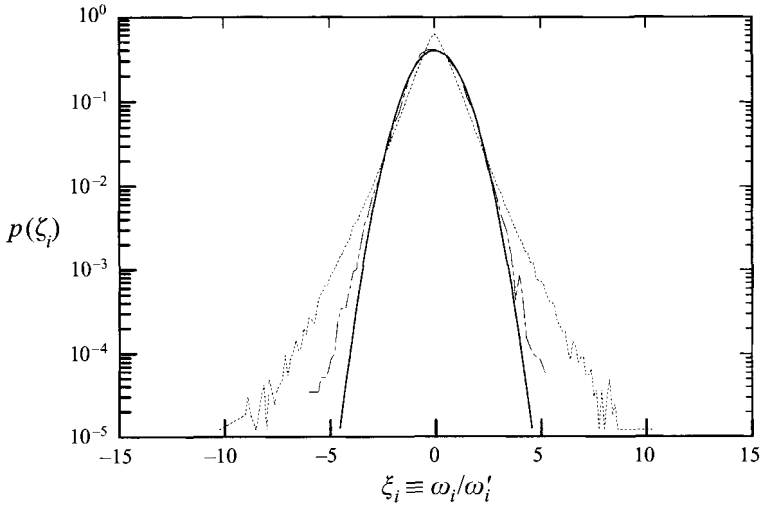

FIGURE 14. Probability density function of ω_i. – - –, $i = 1$, Fan (1991), $R_\lambda = 300$; ···, $i = 3$, present, $R_\lambda = 260$; —, Gaussian distribution with a variance of 1.

the basis of the measurements by Mi & Antonia (1996), it is likely that the present values of F_{ω_2} and F_{ω_3} at $R_\lambda = 120$ and more especially at $R_\lambda = 190$ are underestimated. If this were the case, the rate of increase of F_{ω_i} with R_λ is likely to be greater than that for $F_{u_{1,1}}$; this trend would be consistent with Kerr's (1985) observation that, for $R_\lambda \lesssim 83$, the vorticity flatness factor exponent is the largest of all the fourth-order velocity-derivative moment exponents.

The present corrected Kolmogorov-normalized distribution of $\phi^*_{\omega_3}$ ($R_\lambda = 60$) is compared in figure 16 with the corresponding DNS data of Kim & Antonia (1994) on the centreline ($R_\lambda \simeq 53$) of a fully developed channel flow and the measured data of Ong & Wallace (1995) in a high Reynolds number ($R_\lambda \simeq 870$) turbulent boundary layer. The present distribution falls slightly underneath the DNS spectrum

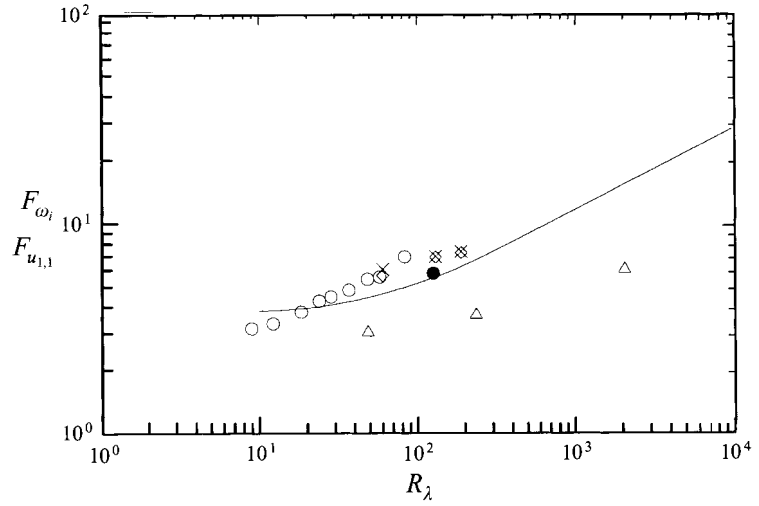

FIGURE 15. Dependence of flatness factors of ω_i and $u_{1,1}$ on R_λ. $i = 1$: ○, DNS (Kerr 1985); △, data collected by Fan (1991); ●, inferred from DNS data of Kida & Murakami (1989). $i = 2$: ◇, present wake data. $i = 3$: ×, present wake data. $F_{u_{1,1}}$: —, best fit to the data of Van Atta & Antonia (1980).

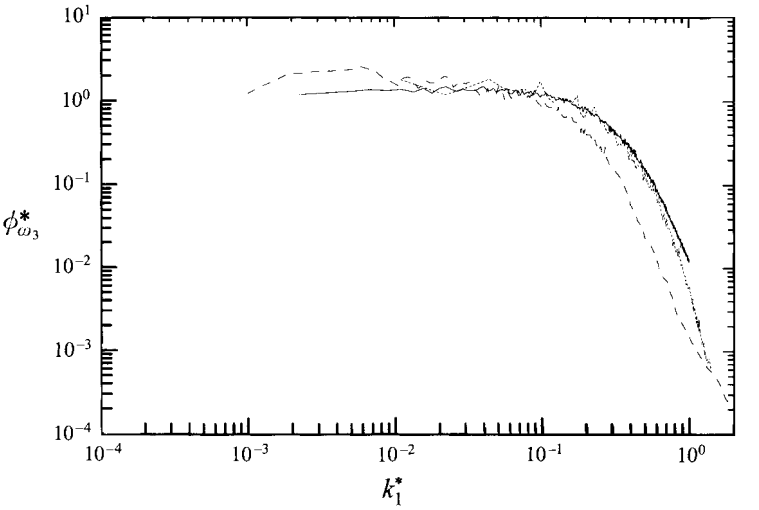

FIGURE 16. $\phi^*_{\omega_3}$ for different flows. —, Present (corrected), $R_\lambda = 60$; ·, DNS, channel flow, $R_\lambda = 53$; - - -, Ong & Wallace (1995), $R_\lambda \simeq 870$.

for $k_1^* \gtrsim 0.4$ but the discrepancy is small, probably within the uncertainty of either the measured or the DNS data. The Ong & Wallace spectrum does however fall away quite sharply, with respect to the other two distributions, for $k_1^* \gtrsim 0.1$. The authors noted that the inadequate spatial resolution of the probe, filtering and noise distorted the data for $k_1^* \gtrsim 0.1$. These data do not therefore invalidate our earlier conclusion (§5) that the high-wavenumber part of the spectrum conforms with Kolmogorov scaling, independently of R_λ. In the inertial range, Ong & Wallace's spectra of ω_i ($i = 1,2,3$) conform with local isotropy, a result which extends our earlier conclusion (§5) in connection with local isotropy in the dissipation range.

9. Conclusions

The lateral components of the vorticity fluctuation were measured just beyond the end of the intermediate wake region of a circular cylinder. The measurements were carried out on the flow centreline at four values of the turbulence Reynolds number R_λ. Particular attention was paid to the high-wavenumber attenuation of the spectrum due to the spatial resolution of the probe. A method for correcting the spectra was developed and applied to the data. Although the correction relies on isotropy, the major contributor to the high-wavenumber part of the lateral vorticity spectrum is the streamwise derivative of the lateral velocity fluctuation. Since the spectral correction for this latter quantity does not rely on the assumption of local isotropy, the correction of the vorticity spectrum is relatively insensitive to this assumption. The assumption has in any case been tested with spectra of the lateral velocity fluctuations and the shear stress cospectrum. The high-wavenumber region of velocity derivatives and vorticity spectra was compared with the appropriate isotropic relations. Overall, agreement with local isotropy is satisfactory over a reasonable wavenumber range ($k_1^* \gtrsim 0.2$). In particular, there is no evidence to suggest that this result depends on R_λ although the range of agreement with isotropy extends to lower wavenumbers when R_λ increases. All the spectra and cospectra show departures from isotropy at low wavenumbers; these departures are reflected in the second- and fourth-order moments of ω_2 and ω_3. In particular, the flatness factors of ω_2 and ω_3 are significantly (30 $\sim$ 40%) larger than the expected isotropic value, namely the flatness factor of $u_{1,1}$. In this context, vorticity fluctuations are more intermittent than fluctuations of $u_{1,1}$, the quantity generally used for quantifying the intermittency of the small-scale structure.

Both spectral and probability density functions of ω_2 and ω_3 evolve with R_λ. For the spectra, the major variation occurs at low wavenumbers with little discernible change at high wavenumbers. For $R_\lambda = 60$, the p.d.f. of ω_2 or ω_3 closely follows a single exponential distribution; this behaviour is replaced by a double exponential behaviour as R_λ increases, the tail of the p.d.f. tending to spread to higher amplitudes. The rate of increase with R_λ of the vorticity flatness factor appears to be larger than that of the $u_{1,1}$ flatness factor. The magnitude of the vorticity flatness factor is larger than that of any of the vorticity components.

At $R_\lambda = 260$, two-point longitudinal correlations of ω_3 provide reasonable support for a '$r^{-4/3}$' inertial range. This behaviour is consistent with the '$r^{2/3}$' inertial-range behaviour of velocity and the isotropic Navier–Stokes equations, when the latter are written in the form of transport equations for two-point vorticity correlation functions.

The support of ARC is gratefully acknowledged.

Appendix. Correction to the ω_3 spectrum

In this Appendix, we provide details for the effect of the spatial resolution on the measured spectra of ω_3 and its components.

The two parallel wires are aligned in the x_3-direction and the inclined wires of the X-probe are in the (x_1,x_2)-plane (note, in figure 1*a*, x_1 is measured from the centre of the probe). The inclined wires are assumed to have an effective angle β and a spanwise separation Δx_3; the separation between the parallel wires is Δx_2 and all wires have a length l. Following Wyngaard (1968), the measured velocity fluctuations

at $\boldsymbol{x}_0$, the location of the probe centre, can be expressed by

$$2u_1^m = u_{1a} + u_{1b} + \cot\beta(u_{2b} - u_{2a}), \tag{A 1}$$

$$2u_2^m = u_{2a} + u_{2b} + \tan\beta(u_{1b} - u_{1a}) \ , \tag{A 2}$$

where the first subscript refers to the velocity fluctuation component; the second subscript denotes the wire (e.g. a, b).

The measured longitudinal derivative $u_{2,1}^m$ can be expressed as

$$u_{2,1}^m = (u_2^m|_{x_0+\Delta x_1} - u_2^m|_{x_0})/\Delta x_1 \ , \tag{A 3}$$

where $\Delta x_1 = -\overline{U}\Delta t$, $\overline{U}$ is the local mean velocity and Δt ($\equiv f_s^{-1}$) is the time between successive samples in the digital time series. The measured lateral derivative $u_{1,2}^m$ can be expressed as

$$u_{1,2}^m = (u_{1c} - u_{1d})/\Delta x_2 \ . \tag{A 4}$$

Fourier–Stieltjes expressions for the velocity fluctuations can be written:

$$u_{1a} = \int_{-\infty}^{+\infty} \mathrm{e}^{\mathrm{i}\boldsymbol{k}\cdot(\boldsymbol{x}_0+\Delta x_3/2)} A_a \mathrm{d}\boldsymbol{Z}_1(\boldsymbol{k}), \tag{A 5}$$

$$u_{2b} = \int_{-\infty}^{+\infty} \mathrm{e}^{\mathrm{i}\boldsymbol{k}\cdot(\boldsymbol{x}_0-\Delta x_3/2)} A_b \mathrm{d}\boldsymbol{Z}_2(\boldsymbol{k}), \tag{A 6}$$

$$u_{1c} = \int_{-\infty}^{+\infty} \mathrm{e}^{\mathrm{i}\boldsymbol{k}\cdot(\boldsymbol{x}_0+\Delta x_2/2)} A \mathrm{d}\boldsymbol{Z}_1(\boldsymbol{k}), \tag{A 7}$$

where $\mathrm{i} = \sqrt{-1}$; $\mathrm{d}\boldsymbol{Z}_1$ and $\mathrm{d}\boldsymbol{Z}_2$ are the Fourier–Stieltjes components of u_1 and u_2, respectively; $\boldsymbol{k}$ is a wavenumber vector with a magnitude of $k \equiv (k_1^2 + k_2^2 + k_3^2)^{1/2}$ while $\Delta \boldsymbol{x_i}$ is a separation vector whose magnitude is Δx_i; A_a, A_b and A are given by

$$A_a = \frac{\sin(\boldsymbol{k}\cdot\boldsymbol{l}_a/2)}{\boldsymbol{k}\cdot\boldsymbol{l}_a/2}, \tag{A 8}$$

$$A_b = \frac{\sin(\boldsymbol{k}\cdot\boldsymbol{l}_b/2)}{\boldsymbol{k}\cdot\boldsymbol{l}_b/2}, \tag{A 9}$$

$$A = \frac{\sin(\boldsymbol{k}\cdot\boldsymbol{l}_c/2)}{\boldsymbol{k}\cdot\boldsymbol{l}_c/2} = \frac{\sin(\boldsymbol{k}\cdot\boldsymbol{l}_d/2)}{\boldsymbol{k}\cdot\boldsymbol{l}_d/2} \ , \tag{A 10}$$

where $\boldsymbol{l}_\alpha$ is the wire length vector of the wire α ($\equiv a, b, c$ and d).

The true and measured ω_3 can be expressed as

$$\omega_3 = \int_{-\infty}^{+\infty} \mathrm{e}^{\mathrm{i}\boldsymbol{k}\cdot\boldsymbol{x}_0/2} \mathrm{d}\boldsymbol{Z}_{\omega_3}, \tag{A 11}$$

$$\omega_3^m = \int_{-\infty}^{+\infty} \mathrm{e}^{\mathrm{i}\boldsymbol{k}\cdot\boldsymbol{x}_0/2} \mathrm{d}\boldsymbol{Z}_{\omega_3}^m \ , \tag{A 12}$$

where

$$\mathrm{d}\boldsymbol{Z}_{\omega_3} = \mathrm{i}k_1 \mathrm{d}\boldsymbol{Z}_2 - \mathrm{i}k_2 \mathrm{d}\boldsymbol{Z}_1 \tag{A 13}$$

and

$$\begin{aligned} \mathrm{d}\boldsymbol{Z}_{\omega_3}^m = \frac{\mathrm{e}^{\mathrm{i}\boldsymbol{k}\cdot\Delta\boldsymbol{x}_1} - 1}{2p} \Big\{ &\left[\mathrm{e}^{\mathrm{i}\boldsymbol{k}\cdot\Delta\boldsymbol{x}_3/2} A_a + \mathrm{e}^{-\mathrm{i}\boldsymbol{k}\cdot\Delta\boldsymbol{x}_3/2} A_b\right] \mathrm{d}\boldsymbol{Z}_2 \\ &+ \tan\beta \left[\mathrm{e}^{-\mathrm{i}\boldsymbol{k}\cdot\Delta\boldsymbol{x}_3/2} A_b - \mathrm{e}^{\mathrm{i}\boldsymbol{k}\cdot\Delta\boldsymbol{x}_3/2} A_a\right] \mathrm{d}\boldsymbol{Z}_1 \Big\} \\ &- 2A\mathrm{i}\sin\frac{\boldsymbol{k}\cdot\Delta\boldsymbol{x}_2}{2} \mathrm{d}\boldsymbol{Z}_1/\Delta x_2 \ . \end{aligned} \tag{A 14}$$

The spectra of ω_3^m and ω_3 are given by

$$\phi^m_{\omega_3}(\boldsymbol{k}) = \overline{\mathrm{d}\boldsymbol{Z}^m_{\omega_3}(\mathrm{d}\boldsymbol{Z}^m_{\omega_3})^\dagger}/\mathrm{d}\boldsymbol{k}, \tag{A 15}$$

$$\phi_{\omega_3}(\boldsymbol{k}) = \overline{\mathrm{d}\boldsymbol{Z}_{\omega_3}(\mathrm{d}\boldsymbol{Z}_{\omega_3})^\dagger}/\mathrm{d}\boldsymbol{k}, \tag{A 16}$$

where the dagger denotes the complex conjugate.

Substitutions of (A 13) and (A 14) into (A 15) and (A 16) yield

$$\phi_{\omega_3}(\boldsymbol{k}) = k_1^2\phi_{22}(\boldsymbol{k}) + k_2^2\phi_{11}(\boldsymbol{k}) - 2k_1k_2\phi_{12}(\boldsymbol{k}), \tag{A 17}$$

$$\begin{aligned}
\phi^m_{\omega_3}(\boldsymbol{k}) = \frac{1-\cos(\boldsymbol{k}\cdot\Delta\boldsymbol{x}_1)}{2\Delta x_1^2}\{&[A_a^2 + 2\cos(\boldsymbol{k}\cdot\Delta\boldsymbol{x}_3)A_aA_b + A_b^2]\phi_{22}(\boldsymbol{k}) \\
&+\tan^2\beta[A_a^2 - 2\cos(\boldsymbol{k}\cdot\Delta\boldsymbol{x}_3)A_aA_b + A_b^2]\phi_{11}(\boldsymbol{k}) \\
&+2\tan\beta(A_b^2 - A_a^2)\phi_{12}(\boldsymbol{k})\} + 4A^2\sin^2\frac{\boldsymbol{k}\cdot\Delta\boldsymbol{x}_2}{2}\phi_{11}(\boldsymbol{k})/\Delta x_2^2 \\
&+2A\tan\beta\sin\frac{\boldsymbol{k}\cdot\Delta\boldsymbol{x}_2}{2}\left\{\left[\sin\left(\boldsymbol{k}\cdot\Delta\boldsymbol{x}_1 + \frac{\boldsymbol{k}\cdot\Delta\boldsymbol{x}_3}{2}\right) - \sin\frac{\boldsymbol{k}\cdot\Delta\boldsymbol{x}_3}{2}\right]A_a\right. \\
&\left.-\left[\sin\left(\boldsymbol{k}\cdot\Delta\boldsymbol{x}_1 - \frac{\boldsymbol{k}\cdot\Delta\boldsymbol{x}_3}{2}\right) + \sin\frac{\boldsymbol{k}\cdot\Delta\boldsymbol{x}_3}{2}\right]A_b\right\}\phi_{11}(\boldsymbol{k})/\Delta x_1\Delta x_2 \\
&-2A\sin\frac{\boldsymbol{k}\cdot\Delta\boldsymbol{x}_2}{2}\left\{\left[\sin\left(\boldsymbol{k}\cdot\Delta\boldsymbol{x}_1 + \frac{\boldsymbol{k}\cdot\Delta\boldsymbol{x}_3}{2}\right) - \sin\frac{\boldsymbol{k}\cdot\Delta\boldsymbol{x}_3}{2}\right]A_a\right. \\
&\left.+\left[\sin\left(\boldsymbol{k}\cdot\Delta\boldsymbol{x}_1 - \frac{\boldsymbol{k}\cdot\Delta\boldsymbol{x}_3}{2}\right) + \sin\frac{\boldsymbol{k}\cdot\Delta\boldsymbol{x}_3}{2}\right]A_b\right\}\phi_{12}(\boldsymbol{k})/\Delta x_1\Delta x_2\,,
\end{aligned} \tag{A 18}$$

where the true cross-spectrum $\phi_{ij}(\boldsymbol{k})$ is assumed to be symmetrical with respect to its indices so that $\phi_{12}(\boldsymbol{k}) = \phi_{21}(\boldsymbol{k})$. Similarly, the true and measured derivative components of ω_3 can also be obtained. The 'true' spectra are given by (2.8), (2.9) and (2.10). The 'measured' spectra may be written as follows:

$$\begin{aligned}
\phi^m_{u_{2,1}}(\boldsymbol{k}) = \frac{1-\cos(\boldsymbol{k}\cdot\Delta\boldsymbol{x}_1)}{2\Delta x_1^2}\{&[A_a^2 + 2\cos(\boldsymbol{k}\cdot\Delta\boldsymbol{x}_3)A_aA_b + A_b^2]\phi_{22}(\boldsymbol{k}) \\
&+\tan^2\beta[A_a^2 - 2\cos(\boldsymbol{k}\cdot\Delta\boldsymbol{x}_3)A_aA_b + A_b^2]\phi_{11}(\boldsymbol{k}) \\
&+2\tan\beta(A_b^2 - A_a^2)\phi_{12}(\boldsymbol{k})\},
\end{aligned} \tag{A 19}$$

$$\phi^m_{u_{1,2}}(\boldsymbol{k}) = 4A^2\sin^2\frac{\boldsymbol{k}\cdot\Delta\boldsymbol{x}_2}{2}\phi_{11}(\boldsymbol{k})/\Delta x_2^2 \tag{A 20}$$

and

$$\begin{aligned}
Co^m_{u_{1,2}u_{2,1}}(\boldsymbol{k}) = &2A\tan\beta\sin\frac{\boldsymbol{k}\cdot\Delta\boldsymbol{x}_2}{2}\left\{\left[\sin\left(\boldsymbol{k}\cdot\Delta\boldsymbol{x}_1 + \frac{\boldsymbol{k}\cdot\Delta\boldsymbol{x}_3}{2}\right) - \sin\frac{\boldsymbol{k}\cdot\Delta\boldsymbol{x}_3}{2}\right]A_a\right. \\
&\left.-\left[\sin\left(\boldsymbol{k}\cdot\Delta\boldsymbol{x}_1 - \frac{\boldsymbol{k}\cdot\Delta\boldsymbol{x}_3}{2}\right) + \sin\frac{\boldsymbol{k}\cdot\Delta\boldsymbol{x}_3}{2}\right]A_b\right\}\phi_{11}(\boldsymbol{k})/\Delta x_1\Delta x_2 \\
&-2A\sin\frac{\boldsymbol{k}\cdot\Delta\boldsymbol{x}_2}{2}\left\{\left[\sin\left(\boldsymbol{k}\cdot\Delta\boldsymbol{x}_1 + \frac{\boldsymbol{k}\cdot\Delta\boldsymbol{x}_3}{2}\right) - \sin\frac{\boldsymbol{k}\cdot\Delta\boldsymbol{x}_3}{2}\right]A_a\right. \\
&\left.+\left[\sin\left(\boldsymbol{k}\cdot\Delta\boldsymbol{x}_1 - \frac{\boldsymbol{k}\cdot\Delta\boldsymbol{x}_3}{2}\right) + \sin\frac{\boldsymbol{k}\cdot\Delta\boldsymbol{x}_3}{2}\right]A_b\right\}\phi_{12}(\boldsymbol{k})/\Delta x_1\Delta x_2\,.
\end{aligned} \tag{A 21}$$

Using the isotropic form of $\phi_{ij}(\boldsymbol{k})$, (2.11), the values of $\phi^m_{u_{2,1}}(k_1)$, $\phi^m_{u_{1,2}}(k_1)$, $Co^m_{u_{1,2}u_{2,1}}(k_1)$ and $\phi^m_{\omega_3}(k_1)$ are obtained by numerically integrating (A 19), (A 20), (A 21) and (A 18) over all values of k_2 and k_3.

REFERENCES

ANTONIA, R. A., ANSELMET, F. & CHAMBERS, A. J. 1986 Assessment of local isotropy using measurements in a turbulent plane jet. *J. Fluid Mech.* **163**, 365–391.

ANTONIA, R. A., BROWNE, L. W. B. & CHAMBERS, A. J. 1984 On the spectrum of the transverse derivatives of the streamwise velocity in a turbulent flow. *Phys. Fluids* **27**, 2628–2631.

ANTONIA, R. A., BROWNE, L. W. B. & FULACHIER, L. 1987 Average wavelength of organised structures in the turbulent far wake of a cylinder. *Exps. Fluids* **5**, 298–304.

ANTONIA, R. A., BROWNE, L. W. B. & SHAH, D. A. 1988*a* Characteristics of vorticity fluctuations in a turbulent wake. *J. Fluid Mech.* **189**, 349–365.

ANTONIA, R. A. & KIM, J. 1994 A numerical study of local isotropy of turbulence. *Phys. Fluids* A **6**, 834–841.

ANTONIA, R. A. & MI, J. 1993*a* Corrections for velocity and temperature derivatives in turbulent flows. *Exps. Fluids* **14**, 203–208.

ANTONIA, R. A. & MI, J. 1993*b* Temperature dissipation in a turbulent round jet. *J. Fluid Mech.* **250**, 531–551.

ANTONIA, R. A. & RAJAGOPALAN, S. 1990 Performance of lateral vorticity probe in a turbulent wake. *Exps. Fluids* **9**, 118–120.

ANTONIA, R. A., SATYAPRAKASH, B. R. & HUSSAIN, A. K. M. F. 1982 Statistics of fine-scale velocity in turbulent plane and circular jets. *J. Fluid Mech.* **119**, 55–80.

ANTONIA, R. A., SHAH, D. A. & BROWNE, L. W. B. 1988*b* Dissipation and vorticity spectra in a turbulent wake. *Phys. Fluids* **31**, 1805–1807.

ANTONIA, R. A., ZHU, Y. & KIM, J. 1993 On the measurement of lateral velocity derivatives in turbulent flows. *Exps. Fluids* **15**, 65–69.

ANTONIA, R. A., ZHU, Y. & KIM, J. 1994 Corrections for spatial velocity derivatives in a turbulent shear flow. *Exps. Fluids* **16**, 411–413.

BALINT, J.-L., WALLACE, J. M. & VUKOSLAVCEVIC, P. 1989 The statistical properties of the vorticity field of a two-stream turbulent mixing layer. *Advances in Turbulence II* (ed. H. H. Fernholz & H. E. Fiedler), pp. 74–78. Springer.

BALINT, J.-L., WALLACE, J. M. & VUKOSLAVCEVIC, P. 1991 The velocity and vorticity vector fields of a turbulent boundary layer. Part 2. Statistical properties. *J. Fluid Mech.* **228**, 53–86.

BATCHELOR, G. K. 1953 *The Theory of Homogeneous Turbulence.* Cambridge University Press.

BROWNE, L. W. B., ANTONIA, R. A. & CHUA, L. P. 1989 Calibration of X-probes for turbulent flow measurements. *Exps. Fluids* **7**, 201–208.

BROWNE, L. W. B., ANTONIA, R. A. & SHAH, D. A. 1987 Turbulent energy dissipation in a wake. *J. Fluid Mech.* **179**, 307–326.

CHAMPAGNE, F. H. 1978 The fine-scale structure of the turbulent velocity field. *J. Fluid Mech.* **86**, 67–108.

CORRSIN, S. & KISTLER, A. L. 1955 Free-stream boundaries of turbulent flows. *NACA Rep.* 1244.

EWING, D., HUSSEIN, H. J. & GEORGE, W. K. 1995 Spatial resolution of parallel hot wire probes for derivative measurements. *Exptl Thermal Fluid Sci.* **11**, 155–173.

FAN, M. 1991 Features of vorticity in fully turbulent flows. PhD thesis, Yale University.

FOSS, J. F. 1979 Transverse vorticity measurements. In *Proc. Dynamic Flow Conference 1978* (ed. B. W. Hansen), pp. 983–1001. DISA.

FOSS, J. F. & WALLACE, J. M. 1989 The measurement of vorticity in transitional and fully developed turbulent flows. In *Advances in Fluid Mechanics Measurements* (ed. M. Gad-el-Hak). Lecture Notes in Engineering, vol. 45, pp. 263–321. Springer.

FRENKIEL, F. N. & KLEBANOFF, P. S. 1975 On lognormality of small-scale structure of turbulence. *Boundary-Layer Met.* **8**, 173–200.

FRENKIEL, F. N., KLEBANOFF, P. S. & HUANG, T. 1979 Grid turbulence in air and water. *Phys. Fluids* **22**, 1606–1617.

HAW, R. C., FOSS, J. K. & FOSS, J. F. 1988 Vorticity based intermittency measurements in a single stream shear layer. In *Advances in Turbulence II* (ed. H. H. Fernholz & H. E. Fiedler), pp. 90–95. Springer.

JIMENEZ, J., WRAY, A. A., SAFFMAN, P. G. & ROGALLO, R. S. 1993 The structure of intense vorticity in isotropic turbulence. *J. Fluid Mech.* **255**, 65–90.

KASTRINAKIS, E. G. & ECKELMANN, H. 1983 Measurement of streamwise vorticity fluctuations in a turbulent channel flow. *J. Fluid Mech.* **137**, 165–186.

KASTRINAKIS, E. G., ECKELMANN, H. & WILLMARTH, W. W. 1979. Influence of the flow velocity on a Kovasznay type vorticity probe. *Rev. Sci. Instrum.* **50**, 759–767.

KERR, R. M. 1985 High-order derivative correlations and the alignments of small-scale structures in isotropic numerical turbulence. *J. Fluid Mech.* **153**, 31–58.

KIDA, S. & MURAKAMI, Y. 1989 Statistics of velocity gradients in turbulence at moderate Reynolds numbers. *Fluid Dyn. Res.* **4**, 347–370.

KIM, J. & ANTONIA, R. A. 1993 Isotropy of the small scales of turbulence at low Reynolds number. *J. Fluid Mech.* **251**, 219–238.

KLEWICKI, J. C. & FALCO, R. E. 1990 On accurately measuring statistics associated with small-scale structure in turbulent boundary layers using hot-wire probes. *J. Fluid Mech.* **219**, 119–142.

KOLMOGOROV, A. N. 1941 Local structure of turbulence in an incompressible fluid for very large Reynolds numbers. *Dokl. Akad. Nauk. SSSR* **30**, 299–303.

KOVASZNAY, L. S. G. 1954 Turbulence measurements in physical measurements. In *Gas Dynamics and Combustion* (ed. R. W. Landenbuerg, B. Lewis, R. N. Pease & H. S. Taylor), vol. 10, p. 213.

KUO, A. Y. & CORRSIN, S. 1971 Experiments on internal intermittency and fine structure distribution functions in fully turbulent fields. *J. Fluid Mech.* **50**, 285–319.

LEMONIS, G. C. 1995 An experimental study of the vector fields of velocity and vorticity in turbulent flows. PhD thesis, Swiss Federal Institute of Technology, Zurich.

MARASLI, B., NGUYEN, P. & WALLACE, J. M. 1993 A calibration technique for multiple-sensor hot-wire probes and its application to vorticity measurements in the wake of a circular cylinder. *Exps. Fluids* **15**, 209–218.

MENEVEAU, C., SREENIVASAN, K. R., KAILASNATH, P. & FAN, M. S. 1990 Joint multifractal measures: theory and applications to turbulence. *Phys. Rev.* A **41**, 894–913.

MI, J. & ANTONIA, R. A. 1996 Vorticity characteristics of the turbulent intermediate wake. *Exps. Fluids* **20**, 383–392.

MI, J. & ANTONIA, R. A. 1994 Scaling of spanwise vorticity in turbulent plane wakes. *Rep.* TN - FM 94/4. Department of Mechanical Engineering, University of Newcastle, NSW.

MONIN, A. S. & YAGLOM, A. M. 1975 *Statistical Fluid Mechanics*, Vol. 2. MIT Press.

ONG, L. 1992 Visualization of turbulent flows with simultaneous velocity and vorticity measurements. PhD thesis, University of Maryland.

ONG, L. & WALLACE, J. M. 1995 Local isotropy of the vorticity field in a boundary layer at high Reynolds number. *Advances in Turbulence V* (ed. R. Benzi), pp. 392–397. Kluwer.

PERRY, A. E., LIM, K. L. & HENBEST, S. M. 1987 An experimental study of the turbulence structure in smooth and rough-wall boundary layers. *J. Fluid Mech.* **177**, 437–466.

PHAN-THIEN, N. & ANTONIA, R. A. 1994 Isotropic Cartesian tensors of arbitrary even orders and velocity gradient correlation functions. *Phys. Fluids* **6**, 3818–3822.

RAJAGOPALAN, S. & ANTONIA, R. A. 1993 Structure of the velocity field associated with the spanwise vorticity in the wall region of a turbulent boundary layer. *Phys. Fluids* A **5**, 2502–2510.

ROSE, W. G. 1966 Results of an attempt to generate a homogeneous turbulent shear flow. *J. Fluid Mech.* **25**, 97–120.

SIGGIA, E. D. 1981 Invariants for the one point vorticity and strain rate correlation functions. *Phys. Fluids* **24**, 1934–1936.

SILVERMAN, B. A. 1968 The effect of spatial averaging on spectrum estimation. *J. Appl. Met.* **7**, 168–172.

SREENIVASAN, K. R. 1995 Small-scale intermittency in turbulence. *Proc. Twelfth Australasian Fluid Mechanics Conference, Sydney* (ed. R. W. Bilger), Vol. 2, pp. 549–556.

TAYLOR, G. I. 1935 Statistical theory of turbulence. *Proc. R. Soc. Lond.* A **151**, 421–478.

TSINOBER, A., KIT, E. & DRACOS, T. 1992 Experimental investigation of the field of velocity gradients in turbulent flows. *J. Fluid Mech.* **242**, 169–192.

VAN ATTA, C. W. 1979 Multi-channel measurements and high-order statistics. In *Proc. Dynamic Flow Conference 1978* (ed. B. W. Hansen), pp. 919–941. DISA.

VAN ATTA, C. W. 1991 Local isotropy of the smallest scales of turbulent scalar and velocity fields. *Proc. R. Soc. Lond.* A **434**, 139–147.

VAN ATTA, C. W. & ANTONIA, R. A. 1980 Reynolds number dependence of skewness and flatness factors of turbulent velocity derivatives. *Phys. Fluids* **23**, 252–257.

VEROLLET, E. 1977 Etude d'une couche limite turbulente avec aspiration et chauffage à la paroi. *Rapport* CEA-R-4861. CEN, Saclay.

WALLACE, J. M. 1986 Methods of measuring vorticity in turbulent flows. *Exps. Fluids* **4**, 61–71.

WALLACE, J. M. & FOSS, J. F. 1995 The measurement of vorticity in turbulent flows. *Ann. Rev. Fluid Mech.* **27**, 467–514.

WALLACE, J. M. & VUKOSLAVCEVIC, P. 1982 Measurement of the structure of the streamwise vorticity field in a turbulent boundary layer. In *Structure of Turbulence in Heat and Mass Transfer* (ed. Z. P. Zaric), pp. 29–41. Hemisphere.

WILLMARTH, W. W. 1979 Nonsteady vorticity measurements : survey and new results. In *Proc. Dynamic Flow Conference 1978* (ed. B. W. Hansen), pp. 1003–1012. DISA.

WYNGAARD, J. C. 1968 Measurement of small-scale turbulence structure with hot wires. *J. Phys.* E: *J. Sci. Instrum.* **1**, 1105–1108.

WYNGAARD, J. C. 1969 Spatial resolution of the vorticity meter and other hot-wire arrays. *J. Phys.* E: *J. Sci. Instrum.* **2**, 983–987.

WYNGAARD, J. C. & PAO, Y. H. 1972 Some measurements of the fine structure of large Reynolds number turbulence. In *Statistical Models of Turbulence.* Lecture Notes in Physics, vol. 12, pp. 384–401. Springer.

YAGLOM, A. M. 1981 Laws of small-scale turbulence in atmosphere and ocean (in Commemoration of the 40th Anniversary of the theory of locally isotropic turbulence). *Izv. Atmos. Oceanic Phys.* **17**, 919–935.

ZHU, Y. & ANTONIA, R. A. 1995*a* Spatial resolution of two X-probes for velocity derivative measurements. *Meas. Sci. & Tech.* **6**, 538–549.

ZHU, Y. & ANTONIA, R. A. 1995*b* Effect of wire separation on the X-probe measurement in a turbulent flow. *J. Fluid Mech.* **287**, 199–223.

ZHU, Y., ANTONIA, R. A. & KIM, J. 1993 Velocity and temperature derivative measurements in the near-wall region of a turbulent duct flow. In *Near Wall Turbulent Flows* (ed. R. M. C. So, C. G. Speziale & B. E. Launder), pp.549–561. Elsevier.